Changes in fluid regime in syn-orogenic sediments during the growth of the south Pyrenean fold and thrust belt

DAVID CRUSET[1], IRENE CANTARERO[1], JAUME VERGÉS[2], CÉDRIC M. JOHN[3], DANIEL MUÑOZ-LÓPEZ[1], ANNA TRAVÉ[1]

[1] Departament de Mineralogia, Petrologia i Geologia Aplicada, Facultat de Ciències de la Terra, Universitat de Barcelona, (UB), Martí i Franquès s/n, 08028, Barcelona, Spain.
d.cruset@ub.edu, i_cantarero@ub.edu, munoz-lopez@ub.edu, atrave@ub.edu

[2] Institut de Ciències de la Terra Jaume Almera, ICTJA-CSIC, Lluís Solé i Sabaris s/n, 08028 Barcelona, Spain.
jverges@ictja.csic.es

[3] Department of Earth Science and Engineering, Imperial College London, SW7 2BP, UK.
cedric.john@imperial.ac.uk

Abstract

The eastern sector of the south Pyrenean fold and thrust belt developed during the Alpine compression and affected Upper Cretaceous to lower Oligocene foreland basin deposits. In this study, we determine the changes in fluid regime and fluid composition during the growth of this fold and thrust belt, integrating petrographic and geochemical data obtained from fracture-filling cements.

Hydrothermal fluids at temperatures up to 154 °C, migrated from the Axial zone to the foreland basin and mixed with connate fluids in equilibrium with Eocene sea-water during lower and middle Eocene (underfilled foreland basin). As the thrust front progressively emerged, low-temperature meteoric waters migrated downwards the foreland basin and mixed at depth with the hydrothermal fluids from middle Eocene to lower Oligocene (overfilled non-marine foreland basin).

The comparison of the fluid flow models from the Southern Pyrenees with other orogens worldwide, seems to indicate that the presence or absence of thick evaporitic units highly control fluid composition during the development of fold and thrust belts. Whereas in thrusts not detached along thick evaporite units, mixed fluids are progressively more depleted in $\delta^{18}O$ and have a lower temperature and lower Fe and Sr contents as the thrust front emerges, in thrust detachments through thick evaporite units, the mixed fluids are enriched in $\delta^{18}O$.

Keywords: Fluid regime; Syn-orogenic sediments; Fractures; South Pyrenean fold and thrust belt

1. <u>Introduction</u>

Geofluids interact with sediments during development of fold and thrust belts. These interactions are responsible of ore deposits precipitation and have an important role during hydrocarbon migration and diagenesis, which affects reservoir quality (Oliver, 1986; Qing and Mountjoy, 1992; Machel and Cavell, 1999; Bitzer et al., 2001; Dewaele et al., 2004; Roure et al., 2005; Evans and Fischer, 2012; Vandeginste et al., 2012; Rodríguez-Morillas et al., 2013).

The geochemical composition of the diagenetic products related to fluid flow (cements) depends on the type of fluid, fluid/rock ratios and host rock composition (Banner, 1995; Swennen et al., 2003; Travé et al., 2007; Swart, 2015). Furthermore, fluids favour propagation of fractures, which act as seals or paths (Reynolds and Lister, 1987; McCaig, 1988; Sibson et al., 1988; Carter et al., 1990; Shackleton et al., 2015). Fluid migration along fractures and rock porosity is induced by tectonics (squeegee-type) and/or topography during the successive stages of fold and thrust belts evolution (Oliver, 1986; Heydari, 1997; Bitzer et al., 2001; Pollyea et al., 2015). Thus, the study of fracture- and porosity-filling cements provide information about changes in fluid regime (e.g. temperature, pressure, burial and fluid composition) and in turn, sheds light on the tectonic history of compressional belts (Banks et al., 1991; Marker and Burkhard, 1992; Bitzer et al., 2001; Roure et al., 2005, 2010).

Studies of the relationships between fluids and deformation in fold and thrust belts worldwide report two general trends regarding to fluid flow. The first trend consists of the progressive depletion in $\delta^{18}O$ of the fluids, which has been related to the increase of the temperature of fluids due to the progressive burial of the studied structures (Dewaele et al., 2004; Travé et al., 2004; Breesch et al., 2009; Vilasi et al., 2009; Vilasi, 2010; Evans et al., 2012; Vandeginste et al., 2012; Beaudoin et al., 2014; Fontana et al., 2014). However, other works relate this depletion to the progressive input of low-temperature meteoric waters into the fluid system, which mixed at depth with fluids with a higher temperature and salinity (Immenhauser et al., 2007; Hausegger et al., 2010; Cruset et al., 2016). The second trend consists of the enrichment in $\delta^{18}O$ of fluids along time due to their interaction with clays (Dewever, 2008; Dewever et al., 2013), although in the Larra/Eaux-chaudes thrust (Jaca Basin) and areas affected by salt tectonics, this enrichment is related to the increase of fluid salinity due to the influence of evaporites (Fischer et al., 2013; Crognier et al., 2017).

The South Pyrenean fold and thrust belt constitutes a well-known example in which the relationships between sequential emplacement of thrust sheets of different ages and syn-tectonic deposits are well-constrained (Muñoz et al., 1986; Vergés and Muñoz, 1990; Burbank et al. , 1992a, b; Vergés, 1993; Vergés et al., 2002; Beamud et al., 2010; Carrigan et al., 2016; Labaume et al., 2016). In addition, works already done on fluid regime evolution in the Southern Pyrenees show the same evolution trends regarding fluid flow than those observed in other fold and thrust belts worldwide (Travé et al., 1997, 1998, 2000, 2007; Caja et al., 2006; Caja and Permanyer, 2008; Lacroix et al., 2011, 2014; Beaudoin et al., 2015; Cruset et al. 2016; Crognier et al., 2017). Consequently, the southern Pyrenees represent an excellent laboratory for the study of the changes in fluid regime during progressive deformation in fold and thrust belts.

In this work we define the changes in fluid regime from the beginning of the emplacement of the South eastern Pyrenean thrust sheets to the end of contraction, using data from the entire pile of superposed thrust sheets (Lower Pedraforca, Vallfogona, L'Escala and Abocador thrusts) within the foreland basin (Vergés, 1993). We determine the origin of fluids from which cements precipitated in fractures and rock porosity, their evolution trends during each stage of deformation and controlling parameters using petrographic and geochemical data (carbon, oxygen and strontium isotopes, clumped isotopes thermometry and elemental composition). The results are integrated with previous studies done in the west central Pyrenees (Ainsa Basin (Travé et al., 1997), Castillo Mayor klippe and Jaca thrust (Lacroix et al., 2014), Larra/Eaux-chaudes thrust (Crognier et al., 2017)) and the eastern Ebro Basin, (El Guix anticline (Travé et al., 2000) and Puig-reig anticline (Cruset et al., 2016)), to constrain the evolution of fluid regime at the scale of the south Pyrenean fold and thrust belt, which finally is compared to other compressional belts.

2. Geological setting

The Pyrenees consist of a doubly verging orogenic belt generated during the continental collision between Iberia and Eurasia plates, from Late Cretaceous to Miocene (Muñoz, 2002; Vergés et al., 2002a) (Fig. 1). This collision resulted from the partial subduction of the Iberian plate beneath the Eurasian plate (Choukroune et al., 1989; Roure et al., 1989; Muñoz, 1992, 2002; Vergés et al., 2002). The previous Mesozoic extensional basins were inverted and an antiformal stack constituted of basement-involved thrust sheets developed in the central part of the chain (Axial zone), acting as a boundary between the North and south Pyrenean fold and thrust belts (Muñoz, 1992) (Fig. 1).

The south Pyrenean fold and thrust belt consists of a sequence of south-verging thrusts emplaced in a piggy-back thrust sequence (Puigdefàbregas et al., 1992) and detached predominantly above Triassic evaporites (Séguret, 1972) and Eocene evaporites deposited in the foreland basin (Vergés et al., 1992: Sans, 2003) (Fig. 2).

The four structures selected for this study are located in the south- eastern Pyrenees (Fig. 1) and are representative of the change from marine to continental conditions during thrust front migration. The oldest structure studied is the Lower Pedraforca thrust sheet (Fig. 2a, 3a), an allochthonous klippe detached in the Keuper facies and emplaced from lower to middle Eocene (Puigdefàbregas et al., 1986; Burbank et al., 1992a). The emplacement of the Lower Pedraforca thrust sheet was under marine conditions, as attested by the syn-orogenic conglomerates of Queralt related to this structure (Vergés, 1993). The second structure is the Vallfogona thrust (Fig. 2a, b, 3a), which is the southern boundary of the Cadí thrust sheet. The activity of this thrust fault started in the middle Eocene under marine conditions and finished during the lower Oligocene under continental conditions (Burbank et al., 1992; Vergés, 1993; Vergés and Burbank, 1996; Haines, 2008). The two youngest structures are the Abocador and L'Escala thrusts (Fig. 2b, 3a), active from middle to upper Eocene and from upper Eocene to lower Oligocene, respectively (Travé et al., 2007; Haines, 2008). These two structures affect the sediments of the Ebro foreland basin, which form the footwall of the Vallfogona thrust, and developed under marine-continental transitional conditions (Travé et al., 2007).

The sediments of the study area range in age between Upper Triassic and Oligocene and consist of pre- and syn-orogenic deposits related to the emplacement of the thrust sequence (Fig. 3b). The Lower Pedraforca thrust sheet is composed of the pre-orogenic Keuper facies, Lias and Dogger limestones and dolostones, Santonian limestones and the syn-orogenic Campanian-Maastrichtian coastal deposits of the Areny Fm., Maastrichtian-Thanetian continental deposits from the Garumnian facies, Ilerdian limestones from the Cadí Fm. and Lutetian-Bartonian conglomerates of the Coubet Fm. (Mey et al., 1968; Vergés, 1993; López-Martínez et al., 1999; Rosell et al., 2001; Oms et al., 2007). The hangingwall of the Vallfogona thrust consists of Cuisian-Lutetian turbiditic deposits of the Vallfogona Fm, which are overlain by the Lutetian evaporites of the Beuda Fm. (Vergés et al., 1998). These turbidites are overthrusting the Lutetian to Bartonian marls of the Banyoles and Igualada Fm. and Priabonian-Rupelian syn-tectonic alluvial sediments of the Berga Fm., indicating that the Vallfogona thrust was active until the lower Oligocene (Burbank et al., 1992b; Haines, 2008; Valero et al., 2014). Further south, two formations are involved in the Abocador and L'Escala thrusts. The hangingwalls of both thrusts are constituted of alluvial and fluvial deposits of the Bellmunt Fm. (upper Lutetian; Moya et al., 1991; Serra-Kiel et al., 2003), whereas the footwalls consist of the

Bartonian deltaic deposits of the Puigsacalm Fm. (Mató et al., 1994; Serra-Kiel et al., 2003).

3. Methodology

In order to characterize the evolution of the fluids involved in the emplacement of the Lower Pedraforca, Vallfogona, Abocador and L'Escala thrusts, 107 polished thin sections made from host rocks and fracture-filling cements precipitated during the Alpine compression were studied using petrographic and geochemical methods.

Petrographic observations were made using optical and cathodoluminescence microscopy. A CL TECHNOSYN Cathodoluminescence device Model 8200 MkII operating at 23 kV and 350 μA gun current was used to distinguish the different generations of cements.

Fluid inclusions were examined in calcite cements to determine salinity and temperature conditions of the mineral-forming fluid. Thick sections were used for petrographic characterization of the fluid inclusions and for microthermometric analyses. Measurements were made on a Linkam THMS-600heating-freezing stage. Fluid inclusions, with a size ranging between 2 and 5 μm, were cooled and heated to temperatures around -150°C and 300°C, respectively. However, the attempt to obtain ice melting and homogenization temperatures from two-phase fluid inclusions (liquid-gas) failed, since changes in bubble volume were not observed.

Carbon-coated polished thin sections were used to analyze major, minor and trace element concentrations on a JEOL JXA-8230 electron microprobe. The microprobe was operated using 20 kV of excitation potential, current intensity of 6 nA for Ca and Mg and 40 nA for Mn, Fe and Sr with a beam diameter of 10 μm. Detection limits are 236 ppm for Ca, 131 ppm for Na, 397 ppm for Mg, 226 ppm for Mn, 78 ppm for Fe and 291 ppm for Sr. Precision on major element analyses averaged a standard error of 6.15% at 2σ confidence levels.

Fracture-filling calcite and carbonate host rocks were sampled for carbon- and oxygen-isotope analysis employing a 400 µm-thick dental drill to extract 60 ± 10 µg of powder from trims. The calcite powder was reacted with 100% phosphoric acid for two minutes at 70^{0}C. The resultant CO_2 was analyzed using an automated Kiel Carbonate Device attached to a Thermal Ionization Mass Spectrometer Thermo Electron (Finnigan) MAT-252 following the method of McCrea (1950). The results were corrected using the standard technique (Craig and Gordon, 1965; Claypool et al., 1980), expressed in ‰ with respect to the VPDB (Vienna Pee Dee Belemnite) standard.

For clumped isotopes thermometry, aliquots (replicates) of three carbonate samples weighing 2-3 mg were measured for three out of five samples (GDV20, GDV30, GDV13, table 1) using an automated line developed at Imperial College (The IBEX: Imperial Batch EXtraction system). In addition, two single measurements of two additional samples (TAB9, STn(3)(2), Table 1) were measured using a manual vacuum line described in Dale et al. (2014). In both cases, samples are dropped in 105 % phosphoric acid maintained at 90°C, and reacted for 10 minutes. The reactant CO_2 is separated from contaminants using a poropak-Q column, and transferred into the bellows of a MAT 253 mass spectrometer from Thermo Scientific. Full characterization of a replicate consists of 8 acquisitions in dual inlet mode with 7 cycles per acquisition. All post-acquisition processing were performed using Easotope, a dedicated software for clumped isotope analysis (John and Bowen, 2016). Δ_{47} values are corrected for isotope fractionation during phosphoric acid digestion using a phosphoric acid correction of 0.069 ‰ at 90°C for calcite following Guo et al. (2009), the data is corrected for non-linearity using the heated gas method (Huntington et al., 2009) and projected into the absolute reference frame of Dennis et al. (2011). Carbonate $\delta^{18}O$ values are calculated using the acid fractionation factors of Kim and O'Neil (1997). Most of the samples were measured at least three times, and the results averaged before being converted to temperatures using the calibration of Kluge et al. (2015); in this case, the error reported represents ± 1 standard error of the means. For two samples (TAB9, STn(3)(2), Table 1), only one measurement was performed and the error reported is ± 1 external standard deviation of a measurement.

For $^{87}Sr/^{86}Sr$ analyses, samples of 100% calcite from veins and host rocks were fully dissolved in 0.5M acetic acid, dried and redissolved in 3M HNO_3. The solid residue resulting from reprecipitation was centrifuged at 4000 rpm during 10 minutes before being charged in chromatographic columns. Samples were analyzed on Re single filament with 1µl of H_3PO_4 1M and 2µl of Ta_2O_5 on a TIMS-Phoenix mass spectrometer. The data acquisition method consists of dynamic multicollection during 10 blocks of 16 cycles each one, with a beam intensity in the ^{88}Sr mass of 3V. Analyses have been corrected for possible interferences of ^{87}Rb.

4. Structural and stratigraphic location of the samples

Seven outcrops were studied and sampled to determine the fluid flow regime in the Lower Pedraforca and Vallfogona thrusts and in the Abocador and L'Escala foreland thrusts (Fig. 3).

In the Lower Pedraforca thrust sheet, two different outcrops were sampled along a 1.5 km long transect composed of the Campanian-Maastrichtian coastal deposits of the Areny Fm. and Maastrichtian-Thanetian continental deposits from the Garumnian facies (Q, Fig.3a, b). This transect consists of three south-verging anticlines formed in the southern sector of the imbricated thrust system forming the Lower Pedraforca thrust sheet. The limbs and hinges of these folds are affected by vug porosity and intense fracturing, which consists of bed-perpendicular joints and reverse and strike-slip faults formed as a result of the background deformation related to the Lower Pedraforca thrust sheet. Fault zones related to the major thrusts forming the imbricate system of the Lower Pedraforca thrust sheet do not outcrop in the studied area.

The Vallfogona thrust was sampled in three different outcrops along its strike (GDV, GDB1-2; Fig. 3). Outcrops GDV and GDB1 are formed of up to 450 m-thick fault zones affecting the Cuisian-Lutetian turbidites of the Vallfogona Fm. and the alluvial sediments of the Berga Fm. (Fig. 3b). Outcrop GDB2 is formed of an up to 40 m-thick fault zone affecting only the Berga Fm (Fig. 3b) and consists of a minor thrust fault related to the activity of the Vallfogona thrust. In the three outcrops, the fault zones are mainly composed of damage zones both in the hangingwall and footwall of the Vallfogona thrust in which vug porosity, bed-parallel slip surfaces and reverse and strike-slip faults are concentrated and filled with calcite cement. Sampled fault cores consist of cm-thick gouges with very scarce calcite veins.

The Abocador thrust (TAB) has been studied in a 200 m-thick fault zone with a 7 meters thick fault core whereas the L'Escala thrust (TES) has been studied in a 150 m-thick fault zone, with less than 1 m thick fault core, in both cases cutting through the alluvial sediments of the Lutetian Bellmunt Fm. and Bartonian deltaic deposits of the Puigsacalm Fm (Fig. 3a, b). The fault cores of both thrusts are composed of clay-rich gouges with small calcite veins. Damage zones comprise almost all the volume of the sampled outcrops and are intensively affected by bed-perpendicular joints and reverse and strike-slip faults filled by calcite cement.

5. <u>Fracture analysis</u>

Rocks involved in the studied structures are affected by bed-parallel slip surfaces, joints, E-W to WSW-ENE trending reverse faults and predominantly NW-SE and NE-SW trending strike-slip faults (Fig. 4). Joints are mostly bed-perpendicular, indicating that they formed during layer-parallel shortening together with bed-parallel slip surfaces (Casini et al., 2011). However, some of the joints in L'Escala thrust cut the Bellmunt and Puigsacalm formations at a constant angle regardless bedding dips, indicating that these fractures formed after folding and thrusting. The high trend and dip dispersion of joints in the Lower Pedraforca thrust sheet in contrast to the Abocador and L'Escala thrusts (Fig. 4) is interpreted that deformation was more intense in the former structure or that it extended during a longer period. Reverse and strike-slip faults in the Lower Pedraforca thrust sheet and in the Vallfogona, Abocador and L'Escala thrusts cut stratification at a high angle regardless bedding dips, suggesting that these fractures formed once strata was already folded and therefore, after development of bed-perpendicular joints. The concentration of these faults in the fault zones of major thrusts and the striae sets measured on their planes (Fig. 4), indicating a tectonic displacement to the south in agreement with the regional trend (Vergés, 1993), suggest that they formed during the activity of the major thrusts.

6. Calcite cements

The integration of textural, petrographic and geochemical data obtained from fracture-filling cements allows to identify three generations of calcite cement for the Lower Pedraforca thrust sheet (Cc1 to Cc3), seven for the Vallfogona thrust (Cc1 to Cc7) and two for the Abocador thrust (Cc1 and Cc2) (Fig. 5). In the L'Escala thrust, three calcite cement generations (Cc1 to Cc3) were already identified (Travé et al., 2007) (Fig. 5).

6.1. Petrology

In the Lower Pedraforca thrust sheet, Cc1 cement is formed of up to 30 µm in size of non-luminescent blocky calcite crystals precipitated in the intergranular and intragranular porosity of the Upper Cretaceous Areny Fm. (Fig. 5). Cement Cc2 consists of up to 1 mm of non- to dull orange luminescent sparite calcite crystals precipitated in vug porosity, joints and reverse and strike-slip faults postdating Cc1 (Fig. 5) and affecting both the Areny Fm. and Paleocene Garumnian facies. Calcite cement Cc3 consists of up to 3 mm of zoned dull brown and dull orange blocky sparite calcite crystals precipitated in vug porosity, reverse and strike-slip faults cutting the previous fractures and vugs (Fig. 5).

In the Vallfogona thrust, calcite cements Cc1, Cc2, Cc3 and Cc4 consist of dull brown to non-luminescent calcite, precipitated in fractures and porosity of the Lutetian Vallfogona turbidites from the hangingwall (Fig. 5). Cement Cc1 is formed of 10-20 µm in size blocky sparite precipitated in the intergranular and intragranular porosity of the turbidite sandstones (Fig. 5). Cc2 is formed of 200 µm to 2 mm blocky and up to 1 mm long fibrous sparite precipitated in bed-parallel slip surfaces, bed-perpendicular joints and vug porosity postdating Cc1 (Fig. 5). Calcite cement Cc3 is formed of up to 1 mm long fibrous calcite precipitated parallel to the walls of thrust faults postdating Cc2 (Fig. 5). Cc4 is formed of 100 µm to 2 mm blocky and up to 1mm long fibrous sparite precipitated in strike-slip and thrust faults postdating Cc3 (Fig. 5). Calcite cement Cc5 precipitated in strike-slip and reverse faults and intergranular porosity of Upper Eocene to Oligocene syn-orogenic alluvial sediments of the Berga Fm. from the thrust footwall (Fig. 5). This cement is formed of up to 100 µm blocky and up to 1 mm long fibrous sparite crystals of bright orange calcite (Fig. 5). The presence of Cc5 cement in sediments younger than those in the hangingwall accounts for a later precipitation with respect to Cc1 to Cc4 cements. Cements Cc6 and Cc7 are formed of up to 10 µm of zoned non-luminescent to bright blocky calcite crystals precipitated in vug porosity cross-cutting Cc4 and Cc5 cements, respectively (Fig. 5). The difference between these two last cements lies in their elemental composition (Fig. 6).

In the Abocador thrust, cement Cc1 precipitated in rock porosity and strike-slip and thrust faults affecting the Lutetian alluvial sediments of the Bellmunt Fm. in the hangingwall and Bartonian marls of the Puigsacalm Fm. in the footwall. Cement Cc2 postdates cement Cc1 and precipitated in some reactivated thrust faults (Fig. 5). Both cements consist of orange to bright orange up to 6 µm blocky calcite and up to 10 µm long and 2 µm thick fibrous calcite associated with celestite and barite (Fig. 5).

In L'Escala thrust, calcite cements Cc1, Cc2 and Cc3 consist of orange to bright orange calcite precipitated in fractures affecting the Bellmunt and Puigsacalm Fms. (Fig. 5). Cc1 cement is formed of up to 2 mm blocky crystals and up to 0.7 mm long and 200 µm thick fibrous sparite precipitated in bed-perpendicular pre-thrust joints and thrust faults (Fig. 5). Calcite cements Cc2 and Cc3 are formed of up to 5 mm long and 2 mm thick fibrous sparite filling post-thrust strike-slip faults and post-thrust NW-SE joints respectively (Fig. 5).

6.2. Geochemistry

6.2.1. Elemental composition

Minimum, maximum and mean Fe, Mg, Sr and Mn contents of the calcite cements precipitated in fractures and rock porosity in the Vallfogona, Abocador and L'Escala thrusts, and together with already published data of the Ainsa Basin (Travé et al., 1997), El Guix anticline (Travé et al., 2000) and Puig-reig anticline (Cruset et al., 2016), are plotted in figure 6 (details in supplementary data), summarizing up to 39 analyzed samples and 747 measures.

The graphic (Fig. 6) shows that the Fe content decreases from the activity of the Molinos thrust (23780 ppm) to the last stages of evolution of the Vallfogona thrust (below the detection limit in cement Cc7), that is, from lower Eocene to lower Oligocene (Fig. 6). However, a final increase in the Fe content (up to 7731 ppm) is observed during the lower Oligocene in calcite cements precipitated in the Guix anticline (Fig. 6). The Sr content also shows a depletion from lower Eocene to lower Oligocene, with values ranging from 8090 ppm in the Arro syncline and Atiart thrust to below the detection limit in the El Guix anticline (Fig. 6). Contrarily, the Mg and Mn contents do not show a specific trend during this time span, with values ranging from 4135 to 1452 ppm and from 4239 to below the detection limit, respectively (Fig. 6).

6.2.2. Carbon and oxygen isotopes

The carbon and oxygen composition of the calcite cements precipitated in the Lower Pedraforca thrust sheet, Vallfogona, Abocador and L'Escala thrusts, together with already published data from the Ainsa Basin (Travé et al., 1997), Castillo Mayor klippe and Jaca thrust (Lacroix et al., 2014), El Guix anticline (Travé et al., 2000) and Puig-reig anticline (Cruset et al., 2016) is presented in Fig. 7, summarizing up to 153 analyzed samples.

6.2.2.1. Lower Pedraforca thrust sheet

Upper Cretaceous marine carbonates from the Areny Fm. show $\delta^{13}C$ values ranging between +1.45 and +1.68 ‰ VPDB and $\delta^{18}O$ values ranging between -4.48 and ‰ -3.20 VPDB (Fig. 7). Palustrine limestones from the Paleocene (Garumnian facies) show $\delta^{13}C$ values ranging between -17.47 and -3.65 ‰ VPDB and $\delta^{18}O$ values ranging between -8.20 and -4.77 ‰ VPDB (Fig. 7).

Due to the small size of calcite cement Cc1, only cements Cc2 and Cc3 were analyzed for carbon and oxygen isotopes analysis. Calcite cement Cc2 shows $\delta^{13}C$ values ranging between -15.18 and -0.38 ‰ VPDB and $\delta^{18}O$ values between -9.21 and -2.61 ‰ VPDB (Fig. 7), similar to its adjacent host rock (Fig. 8). Calcite cement Cc3 shows $\delta^{13}C$ values ranging between +0.84 and +1.71 ‰ VPDB and $\delta^{18}O$ values ranging between -9.86 and -4.39 ‰ VPDB (Fig. 7). Calcite cement Cc3 has $\delta^{13}C$ similar to the Upper Cretaceous Areny Fm. and the Paleocene Garumnian Facies, whereas has $\delta^{18}O$ slightly depleted with respect these host rocks (Fig. 8).

6.2.2.2. Vallfogona thrust

Cuisian marine marls from the hangingwall of the Vallfogona thrust (Vallfogona Fm.) show $\delta^{13}C$ values between -2.56 and -0.26 ‰ VPDB and $\delta^{18}O$ values between -6.94 and -4.72 ‰ VPDB (Fig. 7). One sample of Priabonian-Rupelian palustrine limestones from the footwall of the Vallfogona thrust (Berga Fm.) shows $\delta^{13}C$ values of -2.95 ‰ VPDB and $\delta^{18}O$ values of -7.19 ‰ VPDB (Fig. 7).

Due to the small size of Cc1, Cc6 and Cc7 calcite cements, only Cc2, Cc3, Cc4 and Cc5 calcite cements were analyzed for carbon and oxygen isotopes (Fig. 7). These calcite cements show a progressive depletion in $\delta^{13}C$ and $\delta^{18}O$ from Cc2 to Cc5 (Fig.7). Cc2 calcite cement shows $\delta^{13}C$ values ranging between -3.86 and -1.08 ‰ VPDB and $\delta^{18}O$ ranging between -6.24 and -4.74 ‰ VPDB. Cc3 shows $\delta^{13}C$ values ranging between -0.9 and +0.21 ‰ VPDB and $\delta^{18}O$ between -7.55 and -6.04 ‰ VPDB. Calcite cement Cc4 shows $\delta^{13}C$ values ranging between -1.74 and -1.38 ‰ VPDB and $\delta^{18}O$ between -7.34 and -6.74 ‰ VPDB. Calcite cement Cc5 has $\delta^{13}C$ values between -3.05 and -0.57 ‰ VPDB and $\delta^{18}O$ between -9.95 and -7.56 ‰ VPDB. Calcite cements Cc2 to Cc5 have $\delta^{18}O$ progressively more depleted with respect their adjacent host rocks, whereas the $\delta^{13}C$ do not show a clear trend (Fig. 8).

6.2.2.3. Abocador thrust

Due to their small size, carbonate clasts from the Bellmunt Fm. were not sampled. A detrital carbonate clast from the Bartonian Puigsacalm Fm. (footwall) shows $\delta^{13}C$ of -1.69 ‰ VPDB and $\delta^{18}O$ of -8.05 ‰ VPDB. The carbonate fraction from marls from the Puigsacalm Fm. shows $\delta^{13}C$ of +0.45 ‰ VPDB and $\delta^{18}O$ of -6.73 ‰ VPDB (Fig. 7).

Contrarily to the Vallfogona thrust, calcite cements show depletion in $\delta^{13}C$ and enrichment in $\delta^{18}O$ from Cc1 to Cc2 (Fig. 7, 8). Cc1 calcite cement has $\delta^{13}C$ values between -2.72 and -1.05 ‰ VPDB and $\delta^{18}O$ values between -8.81 and -7.61‰ VPDB (Fig. 7). Calcite cement Cc2 has $\delta^{13}C$ values between -4.19 and -1.46 ‰ VPDB and $\delta^{18}O$ values between -6.9 and -4.98 ‰ VPDB (Fig. 7).

6.2.5.4. L’Escala thrust

The carbonate fraction of marls from the Puigsacalm Fm. (footwall) show $\delta^{13}C$ values between -0.80 and 0 ‰ VPDB and $\delta^{18}O$ values between -7.40 and -6.50 ‰ VPDB (Fig. 7).

In the L’Escala thrust, calcite cements show a progressive depletion in $\delta^{13}C$ and $\delta^{18}O$ from Cc1 to Cc3, like in the Vallfogona thrust (Fig.7, 8). Calcite cement Cc1 has $\delta^{13}C$ values between -2.8 and -1.90 ‰ VPDB and $\delta^{18}O$ values between -8.80 and -8.30 ‰

VPDB (Fig. 7). Calcite cement Cc2 has $\delta^{13}C$ values between -0.60 and -0.50 ‰ VPDB and $\delta^{18}O$ values between -9.50 and -9.20 ‰ VPDB (Fig. 7). Calcite cement Cc3 has $\delta^{13}C$ values between -4 and -3.10 ‰ VPDB and $\delta^{18}O$ values between -14.40 and -12.60 ‰ VPDB (Fig. 7).

6.2.3. Clumped isotopes

For this study, clumped isotopes thermometry has been measured in three calcite cements from the Vallfogona thrust (Fig. 9; Table 1). The results are presented together with data already published from the Puig-reig anticline (Cruset et al., 2016) and two preliminary data from the Abocador thrust and El Guix anticline (Fig. 9; Table 1).

For the Vallfogona thrust, the Δ_{47} values for calcite cements Cc2, Cc4 and Cc5 are 0.463 ± 0.002 ‰, 0.532 ± 0.010 ‰ and 0.527 ± 0.023 ‰, respectively. These values translate into temperatures of 154° ± 2°C (Cc2), 101° ± 6°C (Cc4) and 105° ± 14°C (Cc5) using the equation of Kluge et al. (2015) (Fig. 9). Thus, from clumped isotopes temperatures and the equation of Friedman and O'Neil (1977), the $\delta^{18}O_{fluid}$ for Cc2, Cc4 and Cc5 is +12.12 ± 0.14 ‰, +6.37 ± 0.63 ‰ and +4.22 ± 1.37 ‰ VSMOW respectively (Fig. 9).

In the Puig-reig anticline, the measured Δ_{47} values in calcite cements Cc1 and Cc2 are between 0.548 ± 0.009 ‰ and 0.493 ± 0.0010 ‰ and between 0.574 ± 0.010 ‰ and 0.551 ± 0.004 ‰, respectively. With these values, and from the equations mentioned above, we obtain temperatures ranging between 92° ± 5°C and 129° ± 8°C for Cc1 and between 77 ± 5°C and 93° ± 1°C for Cc2 (Fig. 9) and $\delta^{18}O_{fluid}$ for Cc1 and Cc2 is between +4.7 ± 0.6 and +9.2 ± 0.7‰ VSMOW and between -1.7 ± 0.7 and -0.7 ± 0.3‰ VSMOW respectively (Fig. 9).

In the Abocador thrust, a preliminary measured Δ_{47} of 0.423 ± 0.03 is obtained for calcite cement Cc2, which translates into a temperature of 177 ± 40 °C and a $\delta^{18}O_{fluid}$ of +14.1 ± 4.7‰ VSMOW (Fig. 9).

In the El Guix anticline, a preliminary measured Δ_{47} of 0.487 ± 0.03 is obtained for calcite cement precipitated in a thrust fault affecting the sediments forming this fold (micro fracture stage 2 (mfs2) in Travé et al., 2000). This value translates into a temperature of 117 ± 25 °C and a $\delta^{18}O_{fluid}$ of +7.1 ± 2.5‰ VSMOW (Fig. 9).

6.2.4. Strontium isotopes

The $^{87}Sr/^{86}Sr$ ratios of the calcite cements, celestite, host carbonates and evaporites from the Ainsa Basin (Travé et al., 1997), Vallfogona and L'Escala thrusts, El Guix anticline (Travé et al., 2000) and Puig-reig anticline (Cruset et al., 2016) are presented in Fig. 10(for details see supplementary data). The $^{87}Sr/^{86}Sr$ ratios of the Cuisian evaporites of the eastern sector of the south Pyrenean foreland basin (Carrillo, 2012) and the LOWESS curve (McArthur et al., 2001) are also plotted.

From Lower Eocene to Lower Oligocene an increase of the $^{87}Sr/^{86}Sr$ ratios of calcite cements (from 0.707744 to 0.70933) is observed (Fig. 10). At outcrop scale, the $^{87}Sr/^{86}Sr$ ratios from older to younger cements in the Ainsa Basin and the Vallfogona and L'Escala thrusts also show an increment of the $^{87}Sr/^{86}Sr$ ratios (Fig. 10). In contrast, in the Puig-reig anticline this trend is overturned and in El Guix anticline trends are not observed (Fig. 10).

8. Discussion

In this section, we discuss 1) the type and origin of fluids from which calcite cements precipitated in each structure; 2) the changes of fluid regime at the scale of the south Pyrenean fold and thrust belt from lower Eocene to lower Oligocene; and 3) a conceptual model of fluid flow in fold and thrust belts.

8.1. Type of fluids

The type of fluids that flowed through rock porosity and fractures in the south Pyrenean fold and thrust belt can be determined by using the elemental and isotopic composition of the studied calcite cements (Meyers and Lohman, 1985; Banner and Hanson, 1990).

The $\delta^{13}C$ of the calcite cements in the Lower Pedraforca thrust, Vallfogona thrust, cement Cc2 in L'Escala thrust, Ainsa Basin (Travé et al., 1997), El Guix anticline (Travé et al., 2000), Castillo Mayor klippe and Jaca thrust (Lacroix et al., 2014) and Puig-reig anticline (Cruset et al., 2016) are similar to their adjacent host rocks (Fig. 7, 8), indicating that the fluid system was rock-buffered. In contrast, in the Abocador thrust and in cements Cc1 and Cc3 in L'Escala thrust, the $\delta^{13}C$ of calcite cements shows depletion with respect to their adjacent host rocks up to 3.42‰ VPDB and 3.8‰ VPDB respectively (Fig. 7, 8). This depletion can be explained by the input of organogenic or soil-derived carbon into the fluid system (Irwin et al., 1977; Cerling et al., 1989).

The $\delta^{18}O_{fluid}$ calculated from clumped isotopes temperatures for the Vallfogona thrust (+12.12 ‰ VSMOW for Cc2, +6.37 ‰ VSMOW for Cc4 and +4.22 ‰ VSMOW for Cc5), calcite cement Cc1 in Puig-reig anticline (between +4.7 and +9.2 ‰ VSMOW), calcite cement Cc2 in the Abocador thrust (+14.083 ‰ VSMOW) and El Guix anticline (+7.09 ‰ VSMOW) are within the range of magmatic, metamorphic and formation waters (Taylor, 1987). In the Ainsa Basin, a $\delta^{18}O_{fluid}$ within the same range of composition (between +9.51 and +16 ‰ VSMOW) is calculated from fluid inclusion data of celestite formed within calcite cements precipitated in the Arro syncline (Travé et al., 1998) and from the Equation of Friedman and O'Neil (1977). A magmatic origin for these fluids is discarded since magmatism did not develop during the formation of the Pyrenees. Nevertheless, we have no evidence to differentiate between metamorphic and formation waters. The sulfur isotope composition of celestite crystals formed within calcite cements in the Ainsa Basin indicates the influence of marine connate waters trapped in the rock porosity (Travé et al., 1997). This influence has also been reported in calcite veins in the Castillo Mayor klippe, which are time-equivalent to the first stages of deformation of the Ainsa basin (Lacroix et al., 2014). However, the $^{87}Sr/^{86}Sr$ ratios of all the studied calcite cements are higher than those of Eocene seawater (Fig. 10). This fact can be explained by fluids in contact with clay minerals, the input of an external fluid in contact with

Paleozoic crystalline rocks located at depth of the Axial zone and diluted by connate marine waters with low $^{87}Sr/^{86}Sr$ ratios or from the dissolution of emerged rocks by meteoric fluids (McCaig et al., 1995; Travé et al., 1997). The temperatures measured in the Vallfogona thrust (154°C for Cc2, 101°C for Cc4 and 105°C for Cc5), Puig-reig anticline (between 92°C and 129°C for Cc1 and between 77°C and 90°C for Cc2) and Arro syncline (between 157°C and 183°C) were never reached by burial according to cross sections (Vergés, 1993) and vitrinite reflectance data (Clavell, 1992; Vergés et al., 1998) assuming a geothermal gradient of 25°C km^{-1}, thus indicating a thermal anomaly. Preliminary temperature data from the Abocador thrust (177°C) and El Guix anticline (117°C) also seem to point to the presence of high temperature fluids. These results suggest hydrothermal fluid flow along fault zones in the Vallfogona, Abocador and L'Escala thrusts, background fractures in the Lower Pedraforca thrust sheet and fold-related fractures and intergranular porosity in the Puig-reig and el Guix anticlines, which were connected at depth with basement-involved thrusts in the inner part of the Pyrenees, as has been already reported (Bradbury and Woodwell, 1987; McCaig et al., 1995; Travé et al., 2007). However, the progressive decrease in Sr content (Table 1; Fig. 6) and increase of the $^{87}Sr/^{86}Sr$ ratios (Fig. 10) in the thrust front from the lower Eocene to lower Oligocene, together with the depletion in $\delta^{18}O$ (Fig. 7) and decrease in temperature at outcrop scale in the Ainsa Basin, Vallfogona and L'Escala thrusts and Puig-reig anticline, account for the input of meteoric waters, which mixed at depth with the hydrothermal fluids. The depletion in Fe content and $\delta^{18}O$ from older to younger calcite cements related to the input of meteoric waters has been also observed in the Jaca thrust (Lacroix et al., 2014). The progressive depletion in $\delta^{18}O$ is related to the mixing between hydrothermal and meteoric fluids (Immenhauser et al., 2007), whereas the decrease in Fe content (Fig. 6) could be related to the progressive input of oxidizing meteoric fluids into the system (Froelich et al., 1979; Tucker and Wright, 1990), which may have flowed downwards along faults and joints by topography-driven fluid flow (Bitzer et al., 2001).

By contrast, in the Abocador thrust, there is enrichment in the $\delta^{18}O_{calcite}$ from older to younger cements (Fig. 7). This trend has also been observed in the Santo Domingo anticline (Sierras Exteriores, south western Pyrenees) with $\delta^{18}O_{fluid}$ values between -5 and 0 ‰ VSMOW in Bartonian-Priabonian veins and between +5 and +10 ‰ VSMOW in upper Priabonian-lower Rupelian veins (Crognier et al. 2016). These authors interpret the highest $\delta^{18}O_{fluid}$ values as a strong interaction between meteoric waters and host rocks or by the input of strongly evaporated fluids. In the same area, in the Pico del Águila anticline, post-folding calcite veins precipitated from low-temperature meteoric waters (Beaudoin et al., 2015). From the $\delta^{18}O_{calcite}$ of these veins (from -2.2 to 0 ‰ VPDB) together with the temperatures reported by these authors (below 80 ± 20ºC) a $\delta^{18}O_{fluid}$ between -4 and +11 ‰ VSMOW is obtained, suggesting that these meteoric waters could be highly $\delta^{18}O$-enriched brines. In the Larra/Eaux-chaudes thrust (Jaca Basin), a positive correlation between the $\delta^{18}O_{fluid}$, temperature and salinity is observed from older to younger stages without enrichment in the $\delta^{18}O_{calcite}$ (Crognier et al., 2017). These authors suggest that hydrothermal fluids interacted with Triassic evaporites which acted as the detachment level of the Larra/Eaux-chaudes thrust. A positive correlation between the $\delta^{18}O_{calcite}$ and fluid salinity has also been observed in fracture-filling calcites precipitated in worldwide areas affected by salt tectonics (Fischer et al., 2013).

The same scenario could be suggested for: 1) the Abocador thrust, where preliminary results on clumped isotopes thermometry (177 ± 40 °C and $\delta^{18}O_{fluid}$ of +14.1 ‰ VSMOW) and the presence of barite and celestite associated to calcite cements favor the hypothesis of hydrothermal fluids interacting with brines released from the underlying Eocene evaporites of the Beuda Fm., which acted as the detachment of this structure (Fig. 2b); 2) the El Guix anticline, with calcite cements without systematic $\delta^{18}O$ variation, temperature around 117 ± 25 °C, $\delta^{18}O_{fluid}$ of +7.1 ‰ VSMOW and halite precipitation in thrust zones also favoring the hypothesis of a fluid derived from the underlying Eocene Cardona Salt Formation (Travé et al., 2000) and; 3) the Larra/Eaux chaudes thrust and

Sierras Exteriores with Triassic evaporites acting as the detachment level of the major thrust faults (Labaume et al., 2016). Consequently, we suggest that when evaporitic units are present, the presence of high salinity fluids derived from them, highly controls the $\delta^{18}O$ of the calcite cements.

The presence of the thermal anomalies discussed above, with fluids in disequilibrium with their adjacent host rocks during millions of years, indicate the occurrence of thermal convection controlling fluid flow (Lipsey et al., 2016). According to this mechanism, large volumes of fluids are drived to the reaction site through fractures and permeable host rocks during long time periods (Person et al., 1996; Morrow, 1998). Other scenarios, which involve fluid release by heating or decompression of interstitial fluids by seal breaking are ruled out, since these mechanisms provide low volumes of fluids and they do not generate thermal anomalies (Gomez-Rivas et al., 2014).

8.2. Changes in fluid regime in the south Pyrenean fold and thrust belt from lower Eocene to lower Oligocene

The geochemical signatures of the calcite cements in the Lower Pedraforca thrust sheet, Vallfogona, Abocador and L'Escala thrusts, Ainsa Basin (Travé et al., 1997), Castillo Mayor klippe and Jaca thrust (Lacroix et al., 2014), El Guix anticline (Travé et al., 2000) and Puig-reig anticline (Cruset et al., 2016) with respect to their timing of precipitation (Fig. 11) highlights that hydrothermal fluids have migrated along the south Pyrenean fold and thrust belt from the lower Eocene to lower Oligocene (Fig. 12).

From the lower to middle Eocene, hydrothermal fluids migrated during thrusting along reverse faults, strike-slip faults and joints from the crystalline basement to the syn-orogenic marine sediments deposited in the foreland basin (Fig. 12). During this period, hydrothermal fluids mixed with connate marine waters expelled from rock porosity by sediment compaction during the early stages of evolution of the foreland basin (Bitzer et al., 2001). The resultant fluid had a sulfur isotope composition in equilibrium with Eocene marine waters (Travé et al. 1997), high Fe and Sr contents (Fig. 6), enriched $\delta^{18}O$ (Fig. 7) and had $^{87}Sr/^{86}Sr$ ratios slightly higher than Eocene seawater (Fig. 10).

From the middle Eocene to lower Oligocene, as the foreland basin changed from underfilled to overfilled, the thrust front progressively emerged from deep water to endorheic domains (Fig. 11 and 12). The relative sea-level fall and related change in topographic elevation initiated topography-driven fluid flow (Bitzer et al., 2001) and as a consequence, the influence of meteoric waters, that mixed at depth with hydrothermal ascending fluids, increased progressively and changed the fluid composition (Fig. 12). This change in fluid flow conditions is reflected in the progressive decrease in Fe and Sr contents (Fig. 6), temperature (Table 1), depletion in $\delta^{18}O$ (Fig. 7) and high $^{87}Sr/^{86}Sr$ ratios with respect calcite cements precipitated previously (Fig. 10). However, in other areas such as the Abocador thrust, El Guix anticline (Travé et al., 2000) and the Sierras Exteriores and Larra/Eaux-chaudes thrust (Beaudoin et al., 2015; Crognier, 2016; Crognier et al., 2017), brines derived from the underlying thick evaporite units interacted with hydrothermal and meteoric fluids and controlled fluid composition even when these structures grew under continental conditions.

Assuming that hydrothermal fluid flow was continuous during the activity of the studied structures, the minimum fluid flow rate has been roughly estimated considering that fluids migrated from the basement hanging-wall cut-off to the frontal part of the Lower Pedraforca thrust sheet (30 km), the Vallfogona thrust (20 km where it has been studied; Fig. 2A), the Abocador thrust (24 km) and the L'Escala thrust (24 km) during 6, 11, 5 and 8 Ma, respectively. These ranges of time are based on magnetostratigraphy and $^{40}Ar/^{39}Ar$ dating on authigenic illite on fault planes (Vergés, 1993; Haines, 2008). Thus, for the Lower Pedraforca thrust sheet and the Abocador thrust, a minimum fluid flow rate of 5 km Ma^{-1} is obtained, whereas for the Vallfogona and the L'Escala thrusts the minimum calculated rate is 2 and 3 km Ma^{-1}, respectively. These values are consistent with the lowest rates calculated in other forelands such as in the Canadian and eastern

Venezuelan foothills (Schneider, 2003) and in the Bighorn Basin (Beaudoin et al., 2014). This large-scale migration of hydrothermal fluids along the south Pyrenean fold and thrust belt was probably controlled by different driving forces such as squeegee-type fluid flow, which induces rates between 1 and 100 km Ma^{-1} (Ge and Garven, 1989) but only during short time periods (Schneider, 2003), coupled with topography and thermal gradients (Lyubetskaya and Ague, 2009).

8.3. Conceptual model of fluid flow in fold and thrust belts

The fluid flow model established for the southern Pyrenees in the previous section together with previous works done by other authors in other orogens worldwide (Ferket et al., 2000; Van Geet et al., 2002; Breesch, 2008; Vilasi, 2010; Vandeginste et al., 2012; Dewever et al., 2013), indicate that the presence or absence of thick evaporitic units highly control the final fluid composition. In all cases, ascending hydrothermal fluids mixed with low-temperature meteoric fluids (Fig. 13).

However, whereas in thrust sheets not detached along evaporite units (Fig. 13a), the mixed fluid was progressively more depleted in $\delta^{18}O$ and had lower Fe and Sr contents with respect to the former, not mixed, hydrothermal fluid (Fig. 13a), in thrust sheets detached along evaporite successions (Fig. 13b), brines derived from these evaporites were responsible for the $\delta^{18}O$ enrichment of the mixed fluid, without a systematic increase in Fe and Sr contents (Warren, 2006).

The trend from high $\delta^{18}O$ to more depleted values along with, where documented, the progressive decrease in Fe and Sr contents (Fig. 13a) during the emersion of the thrust front has been observed in the Vallfogona and L'Escala thrust, Ainsa Basin (Travé et al., 1997), Veracruz Basin (Ferket et al., 2000), North Oman Mountains (Breesch, 2008), south Ionian zone (Vilasi, 2010), Canadian Rocky Mountains (Vandeginste et al., 2012), Bighorn Basin (Beaudoin et al., 2011, 2014), Castillo Mayor klippe and Jaca thrust (Lacroix et al., 2014) and Puig-reig anticline (Cruset et al., 2016), which are structures not detached through thick evaporite units. As these structures emerged, the input of oxidizing meteoric waters depleted in Sr controlled the decrease in Fe content (Froelich et al., 1979; Tucker and Wright, 1990), whereas their mixing with hydrothermal fluids induced $\delta^{18}O$ depletion (Immenhauser et al., 2007). The trend from low $\delta^{18}O$ to more enriched values (Fig. 13b) has been observed in the Abocador thrust, El Guix anticline (Travé et al., 2000), Central Ionian Zone (Van Geet et al., 2002), Sicilian fold and thrust belt (Dewever et al., 2013), Sierras Exteriores (Beaudoin et al., 2015; Crognier et al., 2015; Crognier, 2016) and Larra/Eaux chaudes thrust (Crognier et al., 2017), where thrusts are detached along thick evaporitic units. In the Iudica-Scalpello area (Sicilian fold and thrust belt), based on the low salinity of the fluid inclusions, this trend is explained by smectite-illite transformations (Dewever et al., 2013).

9. <u>Conclusions</u>

A multidisciplinary study has been carried out to determine the changes in fluid regime and composition during the growth of the south Pyrenean fold and thrust belt from lower Eocene to lower Oligocene.

Integration of petrographic and geochemical data obtained from fracture-filling calcite cements reveals that hydrothermal fluids migrated from the Axial zone of the Pyrenees to its related foreland basin during Paleogene compression.

From Lower to Middle Eocene, ascending hydrothermal fluids migrated from the Axial zone to the foreland basin and mixed with connate marine waters trapped in rock porosity. The mixed fluid had temperatures up to 154 °C, enriched $\delta^{18}O$, $^{87}Sr/^{86}Sr$ slightly higher than Eocene seawater and high Fe and Sr contents. From Middle Eocene to Lower Oligocene, as the thrust front progressively emerged, meteoric waters migrated downwards the foreland basin by topography-driven fluid flow and mixed at depth with the hydrothermal fluids. The mixed fluid was progressively more depleted in $\delta^{18}O$, with temperatures between 77 and 129°C, lower Fe and Sr contents and more radiogenic $^{87}Sr/^{86}Sr$ ratios than the former fluid.

The comparison of southern Pyrenees to other orogens worldwide, suggests that the presence or absence of thick evaporitic units had a fundamental role in the fluid composition during fold and thrust belt evolution. In all cases, hydrothermal fluids migrated along fractures within thrust sheets and mixed with low-temperature meteoric waters. When thrusts were not detached through thick evaporite units, the resultant fluid was progressively more radiogenic, more depleted in $\delta^{18}O$ and had a lower temperature and lower Sr and Fe content, as the thrust front emerged. In contrast, when thrusts were detached along thick evaporitic units, the resulting fluid was enriched in $\delta^{18}O$.

Acknowledgements

The Isotopic and electron microprobe analyses were carried out at “Centres Científics i Tecnològics” of the Universitat de Barcelona. Strontium analyses were done at the “CAI de Geocronología y Geoquímica Isotópica (UCM-CEI)” of the Universidad Complutense de Madrid. The clumped isotopes analyses were performed in the Qatar Stable Isotope Laboratory of Imperial College of London. This research was performed within the framework of DGICYT Spanish Project CGL2015-66335-C2-1-R and ALPIMED Project (PIE-CSIC-201530E082), Grup Consolidat de Recerca “Geologia Sedimentària” (2014SGR-251). We thank Pierre Labaume and Nicolas Beaudoin for their constructive reviews which highly improved the quality of the manuscript.

References

Banks, D.A., Davies, G.R., Yardley, B.W.D., McCaig, A.M. and Grant, N.T., 1991. The chemistry of brines from an Alpine thrust system in the Central Pyrenees: An application of fluid inclusion analysis to the study of fluid behavior in orogenesis. Geochimia et Cosmochimica Acta, 55, 1021-1030.

Banner, J.L., 1995. Application of the trace element and isotope geochemistry of strontium to studies of carbonate diagenesis. Sedimentology, 42, 805-824.

Banner, J.L. and Hanson, G.N., 1990. Calculation of simultaneous isotopic and trace element variations during water-rock interaction with applications to carbonate diagenesis. Geochimia et Cosmochimica Acta, 54, 3123-3137.
Beamud, E., Muñoz, J.A., Fitzgerald, P.G., Baldwin, S.L., Garcés, M., Cabrera, L. and Metcalf, J.R., 2010. Magnetostratigraphy and detrital apatite fission track thermochronology in syntectonic conglomerates: constraints on the exhumation of the South-Central Pyrenees. Basin Research, 23(3), 309-331.
Beaudoin, N., Bellahsen, N., Lacombe, O. and Emmanuel, L., 2011. Fracture-controlled paleohydrogeology in a basement-cored, fault-related fold: Sheep Mountain Anticline, Wyoming, United States. Geochemistry, Geophysics, Geosystems, 12(6), 1-15.
Beaudoin, N., Bellahsen, N., Lacombe, O., Emmanuel, L. and Pironon, J., 2014. Crustal-scale fluid flow during the tectonic evolution of the Bighorn Basin (Wyoming, USA). Basin Research, 26(3), 403-435.
Beaudoin, N., Huyghe, D., Bellahsen, N., Lacombe, O., Emmanuel, L., Mouthereau, F. and Ouanhnon, L., 2015. Fluid systems and fracture development during syn-depositional fold growth: An example from the Pico del Aguila anticline, Sierras Exteriores, southern Pyrenees, Spain. Journal of Structural Geology, 70, 23-38.
Bitzer, K., Travé, A. and Carmona, J.M., 2001. Fluid flow processes at basin scale. Acta Geologica Hispanica, 36(1-2), 1-20.
Bradbury, H.J. and Woodwell, G.R., 1987. Ancient fluid flow within foreland terrains. In: J.C. Goff and B.P.J. Williams (Eds.), Fluid flow in Sedimentary Basins and Aquifers. Geological Society Special Publication, pp. 87-102.
Breesch, L., 2008. Diagenesis and fluid system evolution in the Northern Oman Mountains, United Arab Emirates, PhD thesis, Katholieke Universiteit Leuven, Leuven, Belgium, 159 pp.
Breesch, L., Swennen, R. and Vincent, B., 2009. Fluid flow reconstruction in hanging and footwall carbonates: Compartmentalization by Cenozoic reverse faulting in the Northern Oman Mountains (UAE). Marine and Petroleum Geology, 26, 113-128.
Burbank, D.W., Puigdefàbregas, C. and Muñoz, J.A., 1992a. The chronology of the Eocene tectonic and stratigraphic development of the Eastern Pyrenean Foreland Basin. NE Spain. Geol. Soc. America Bull., 104, 1101-1120.
Burbank, D.W., Vergés, J., Muñoz, J.A. and Bentham, P., 1992b. Coeval hinward- and forward-imbricating thrusting in the south-central Pyrenees, Spain: Timing and rates of shortening and deposition. Geological Society of America Bulletin, 104, 3-17.
Caja, M.A. and Permanyer, A., 2008. Significance of organic matter in Eocene turbidite sediments (SE Pyrenees, Spain). Naturwissenschaften, 9, 1073-1077.
Caja, M.A., Permanyer, A., Marfil, R., Al-Asm, I.S. and Martín-Crespo, T., 2006. Fluid flow record from fracture-fill calcite in the Eocene limestones from the South-Pyrenean Basin (NE Spain) and its relationship to oil shows. Journal of Geochemical Exploration, 89, 27-32.
Carrigan, J.H., Anastasio, D.J., Kodama, K.P. and Parés, J.M., 2016. Fault-related fold kinematics recorded by terrestrial growth strata, Sant Llorenç de Morunys, Pyrenees Mountains, NE Spain. Journal of Structural Geology, 91, 161-176.
Carrillo, E., 2012. The Evaporites of the Southeastern Pyrenean Basin (Late Cuisian – Lutetian): Sedimentology and Structure, PhD Thesis, University of Barcelona, Barcelona, Spain, 192 pp.
Carter, N.L., Kronenberg, A.K., Ross, J.V. and Wiltschko, D.V., 1990. Control of fluids on deformation of rocks. In: R.J. Knipe and E.H. Rutter (Eds.), Deformation Mechanisms, Rheology and Tectonics. Geological Society, London, Special Publications, pp. 1-13.
Casini, G., Gillespie, P.A., Vergés, J., Romaire, I., Fernández, N., Casciello, E., Saura, E., Mehl, C., Homke, S., Embry, J.-C., Aghajari, L. and Hunt, D.W., 2011. Sub-seismic fractures in Foreland fold and Thrust belts: insight from the Lurestan Province, Zagros Mountains, Iran. Petroleum Geoscience, 17, 263-282.

Cerling, T.E., Quade, J., Wang, Y. and Bowman, J.R., 1989. Carbon isotopes in soils and palaeosols as ecology and palaeoecology indicators. Nature, 341, 138-139.

Clavell, E., 1992. Geologia del petroli de les conques terciàries de Catalunya, PhD thesis, University of Barcelona, 488 pp.

Claypool, G.E., Kaplan, W.T., Kaplan, I.R., Sakai, H. and Zak, I., 1980. The age curves of sulfur and oxygen isotopes in marine sulfate and their mutual interpretations. Chemical Geology, 28, 199-260.

Costa, E., Garcés, M., López-Blanco, M., Beamud, E., Gómez-Paccard, M. and Larrasoaña, J.C., 2010. Closing and continentalization of the South Pyrenean foreland basin (NE Spain): magnetochronological constraints. Basin Research, 22(6), 904-917.

Craig, H. and Gordon, I.-I., 1965. Deuterium and oxygen-18 variations in the ocean and the marine atmosphere. In: E. Tongiorgi (Ed.), Proceedings of a Conference on Stable Isotopes in Oceanographic Studies and Paleotemperatures. Consiglio Nazionale delle Richerche, Laboratorio di Geologia Nucleare, Pisa, Italy, pp. 9-130.

Crognier, N., Hoareau, G., Aubourg, C., Dubois, M., Lacroix, B., Branellec, M., Callot, J.P. and Vennemann, T., 2017. Syn-orogenic fluid flow in the Jaca basin (south Pyrenean fold and thrust belt) from fracture and vein analyses. Basin Research, 1-30.

Cruset, D., Cantarero, I., Travé, A., Vergés, J. and John, C.M., 2016. Crestal graben fluid evolution during growth of the Puig-reig anticline (South Pyrenean fold and thrust belt). Journal of Geodynamics, 101, 30-50.

Choukroune, P. and team, E., 1989. The ECORS Pyrenean deep seismic profile reflection data and the overall structure of an orogenic belt. Tectonics, 8, 23-39.

Dale, A., John, C.M., Mozley, P.S., Smalley, P.C. and Muggeridge, A.H., 2014. Time-capsule concretions: Unlocking burial diagenetic processes in the Mancos Shale using carbonate clumped isotopes. Earth and Planetary Science Letters, 394, 30-37.

Dennis, K.J., Affeck, H.P., Passey, B.H., Schrag, D.P. and Eiler, J.M., 2011. Defining an absolute reference frame for 'clumped' isotope studies of CO2. Geochimia et Cosmochimica Acta, 75(22), 7117-7131.

Dewaele, D., Muchez, P. and Banks, D.A., 2004. Fluid evolution along multistage composite fault systems at the southern margin of the Lower Palaeozoic Anglo-Brabant fold belt, Belgium. Geofluids, 4, 341-356.

Dewever, B., 2008. Diagenesis and fluid flow in the Sicilian fold-and-thrust bellt, PhD thesis. Katholieke Universiteit Leuven, Leuven, Belgium, 183 pp.

Dewever, B., Swennen, R. and Breesch, L., 2013. Fluid flow compartmentalization in the Sicilian fold and thrust belt: Implications for the regional aqueous fluid flow and oil migration history. Tectonophysics, 591, 194-209.

Evans, M.A., Bebeout, G.E. and Brown, C.H., 2012. Changing fluid conditions during folding: An example from the central Appalachians. Tectonophysics, 576-577, 99-115.

Evans, M.A. and Fischer, M.P., 2012. On the distribution of fluids in folds: A review of controlling factors and processes. Journal of Structural Geology, 44, 2-24.

Ferket, H., Roure, F., Swennen, R. and Ortuño, S., 2000. Fluid migration placed into the deformation history of fold-and-thrust belts: an example from the Veracruz basin (Mexico). Journal of Geochemical Exploration, 69-70, 275-279.

Fischer, M.P., Kenroy, P.R. and Smith, A.P., 2013. Fluid Systems around Salt Diapirs, AAPG Annual Convention and Exhibition, Pittsburgh, Pennsylvania, May 19-22, 2013.

Fontana, S., Nader, F.H., Morad, S., Ceriani, A., Al-Aasm, I.S., Daniel, J.-M. and Mengus, J.-M., 2014. Fluid–rock interactions associated with regional tectonics and basin evolution. Sedimentology, 61(3), 660-690.

Friedman, I. and O'Neil, J.R., 1977. Compilation of stable isotope fractionation factors of geochemical interest. In: M. Fleischer (Ed.), Data of Geochemistry, U. S. Gov. Print. Off. Washington D. C., pp. 1-12.

Froelich, P.N., Klinkhammer, G.P., Bender, M.L., Luedtke, N.A., Heath, G.R., Cullen, D., Dauphin, P., Hammond, D., Hartman, B. and Maynard, V., 1979. Early oxidation of organic matter in pelagic sediments of the eastern equatorial Atlantic: suboxic diagenesis. Geochimia et Cosmochimica Acta, 43, 1075-1090.

Ge, S. and Garven, G., 1989. Tectonically Induced Transient Groundwater Flow in Foreland Basin. In: R.A. Price (Ed.), Origin and Evolution of Sedimentary Basins and Their Energy and Mineral Resources. American Geophysical Union, pp. 145-157.

Geet, M.V., Swennen, R., Durmishi, C., Roure, F. and Muchez, P., 2002. Paragenesis of Cretaceous to Eocene carbonate reservoirs in the Ionian fold and thrust belt (Albania): relation between tectonism and fluid flow. Sedimentology, 49, 697-718.

Gomez-Rivas, E., Corbella, M., Martín-Martín, J.D., Stafford, S.L., Teixell, A., Bons, P.D., Griera, A. and Cardellach, E., 2014. Reactivity of dolomitizing fluids and Mg source evaluation of fault-controlled dolomitization at the Benicàssim outcrop analogue (Maestrat basin, E Spain). Marine and Petroleum Geology, 55, 26-42.

Guo, W., Mosenfelder, J.L., Goddard, W.A. and Eiler, J.M., 2009. Isotopic fractionations associated with phosphoric acid digestion of carbonate minerals: Insights from first-principles theoretical modeling and clumped isotope measurements. Geochimia et Cosmochimica Acta, 73(24), 7203-7225.

Haines, S.H., 2008. Transformations in Clay-Rich Fault Rocks: Constraining Fault Zone Processes and the Kinematic Evolution of Regions, PhD thesis. University of Michigan, Ann Arbor, U.S. , 295 pp.

Hausegger, S., Kurz, W., Rabitsch, R., Kiechl, E. and Brosch, F.-J., 2010. Analysis of the internal structure of a carbonate damage zone: Implications for the mechanisms of fault breccia formation and fluid flow. Journal of Structural Geology, 32(9), 1349-1362.

Heydari, E., 1997. Hydrotectonic models of burial diagenesis in platform carbonates based on formation water geochemistry in North American sedimentary basins. In: I.P. Montañez, J.M. Gregg and K.L. Shelton (Eds.), Basin-wide diagenetic patterns: integrated petrologic, geochemical, and hydrologic considerations. Society of Economic Paleontologists and Mineralogists, Special Publication 57, pp. 53-79.

Huntington, K.W., Eiler, J.M., Affek, H.P., Guo, W., Boniface, M., Yeung, L.Y., Thiagarajan, N., Passey, B., Tripati, A., Daëron, M. and Came, R., 2009. Methods and limitations of 'clumped' CO2 isotope (Δ47) analysis by gas-source isotope ratio mass spectrometry. Journal of Mass Spectrometry, 44(9), 1318-1329.

Immenhauser, A., Dublyansky, Y.V., Verwer, K., Fleitman, D. and Pashenko, S.E., 2007. Textural, elemental and isotopic characteristics of Pleistocene phreatic cave deposits (Jabal Madar, Oman). Journal of Sedimentary Research, 77(1-2), 68-88.

Irwin, H., Curtis, C. and Coleman, M., 1977. Isotopic evidence for source of diagenetic carbonates formed during burial of organic-rich sediments. Nature, 269, 209-213.

John, C.M. and Bowen, D., 2016. Community software for challenging isotope analysis: First applications of "Easotope" to clumped isotopes. Rapid Communications in Mass Spectrometry, 30(21), 2285-2300.

Kim, S.T. and O'Neil, J.R., 1997. Equilibrium and nonequilibrium oxygen isotope effects in synthetic carbonates. Geochimia et Cosmochimica Acta, 61(16), 3461-3475.

Kluge, T., John, C.M., Jourdan, A.L., Davis, S. and Crawshaw, J., 2015. Laboratory calibration of the calcium carbonate clumped isotope thermometer in the 25-250 ºC temperature range. Geochimia et Cosmochimica Acta, 157, 213-227.

Labaume, P., Meresse, F., Joliver, M., Teixell, A. and Lahfid, A., 2016. Tectonothermal history of an exhumed thrust-sheet-top basin: An example from the south Pyrenean thrust belt. Tectonics, 35, 1280-1313.

Lacroix, B., Buatier, M., Labaume, P., Travé, A., Dubois, M., Charpentier, D., Ventalon, S. and Convert-Gaubier, D., 2011. Microtectonic and geochemical characterization of thrusting in a foreland basin: Example of the South-Pyrenean orogenic wedge (Spain). Journal of Structural Geology, 33, 1359-1377.

Lacroix, B., Travé, A., Buatier, M., Labaume, P., Vennemann, T. and Dubois, M., 2014. Syntectonic fluid-flow along thrust faults: Example of the South-Pyrenean fold-and-thrust belt. Marine and Petroleum Geology, 49, 84-98.

Lipsey, L., Pluymaekers, M., Goldberg, T., Oversteeg, K.v., Ghazaryan, L., Cloetingh, S. and Wees, J.-D.v., 2016. Numerical modelling of thermal convection in the Luttelgeest carbonate platform, the Netherlands. Geothermics, 64, 135-151.

López-Martínez, N., Fernández-Marrón, M.T. and Valle, M.F., 1999. The succession of vertebrates and plants across the Cretaceous-Tertiary boundary in the Tremp Formation, Ager valley (south-central Pyrenees, Spain). Geobios, 32(4), 617-627.

Lyubetskaya, T. and Ague, J.J., 2009. Modeling the Magnitudes and Directions of Regional Metamorphic Fluid Flow in Collisional Orogens. Journal of Petrology, 50(8), 1505-1531.

Machel, H.G. and Cavell, P.A., 1999. Low-flux, tectonically-induced sequeegee fluid flow ("hot flash") into the Rocky Mountain Foreland Basin. Bulletin of Canadian Petroleum Geology, 47(4), 510-533.

Marker, D. and Burkhard, M., 1992. Fluid circulation, progressive deformation and mass-transfer processes in the upper crust: the example of basement-cover relationships in the External Crystalline Massifs, Switzerland. Journal of Structural Geology, 14(8-9), 1047-1057.

Mató, E., Saula, E., Martínez-Rius, A., Muñoz, J.A. and Escuer, J., 1994. Memoria de la Hoja nº 293 (Berga). Mapa Geológico de España E. 1:50.000 (MAGNA), Segunda Serie, Primera Edición. IGME, 66.

McArthur, J.M., Howarth, R.J. and Bailey, T.R., 2001. Strontium Isotope Stratigraphy: LOWESS Version 3: Best Fit to the Marine Sr-Isotope Curve for 0–509 Ma and Accompanying Look-up Table for Deriving Numerical Age. Journal of Geology, 109, 155-170.

McCaig, A.M., 1988. Deep fluid circulation in fault zones. Geology, 16, 867-870.

McCaig, A.M., Wayne, D.M., Marshall, J.D., Banks, D. and Henderson, I., 1995. Isotopic and fluid inclusion studies of fluid movement along the Gavarnie Thrust, central Pyrenees: Reaction fronts in carbonate mylonites. American Journal of Science, 295, 309-343.

McCrea, J.M., 1950. On the Isotopic Chemistry of Carbonates and a Paleotemperature Scale. Journal of Chemical Physics, 18, 849-957.

Mey, P.H.W., Nagtegaal, P.J.C., Roberti, K.J. and Hartevelt, J.J.A., 1968. Lithostratigraphic subdivision of post-Hercinian deposits in the south-central Pyrenees, Spain. Leidse Geologische Mededelingen, 41, 21-228.

Meyers, W.J. and Lohmann, K.C., 1985. Isotope geochemistry of regionally extensive calcite cement zones and marine components in Mississipian limestones, New Mexico. In: O.M. Harris and N. Schneidermann (Eds.), Carbonate Cements SEPM, Special Publications, pp. 223-239.

Morrow, D.W., 1998. Regional Subsurface dolomitization: models and constraints. Geoscience Canada, 25, 57-70.

Moya, S., Ramos-Guerrero, E., Agustí, J. and Checa, L., 1991. Depositos lacustre-palustres asociados a las zonas intermedias de la Fm. Bellmunt (Prepirineo catalán). I Congreso del Grupo Español del Terciatrio. Comunicaciones, 225-228.

Muñoz, J.A., 1992. Evolution of a continental collision belt: ECORS–Pyrenees crustal balanced section. In: K.R. McClay (Ed.), Thrust Tectonics. Chapman & Hall, London, pp. 235-246.

Muñoz, J.A., 2002. The Pyrenees. In: W. Gibbons and T. Moreno (Eds.), The Geology of Spain. Geological Society, London, pp. 370-385.

Muñoz, J.A., Martínez, A. and Vergés, J., 1986. Thrust sequences in the eastern Spanish Pyrenees. Journal of Structural Geology, 8(3-4), 399-405.

Oliver, J., 1986. Fluids expelled tectonically from orogenic belts: their role in hydrocarbon migration and other geologic phenomena. Geology, 14, 99-102.

Oms, O., Dinarés-Turell, J., Vicens, E., Estrada, R., Vila, B., Galobart, À. and Bravo, A.M., 2007. Integrated stratigraphy from the Vallcebre Basin (southeastern Pyrenees, Spain): New insights on the continental Cretaceous–Tertiary transition in southwest Europe. Palaeogeography, Palaeoclimatology, Palaeoecology, 255, 35-47.

Person, M., Raffensperger, J.P., Ge, S. and Garven, G., 1996. Basin-scale hydrogeologic modeling. Reviews of Geophysics, 34, 61-87.

Pollyea, R.M., Dusen, E.W.V. and Fischer, M.P., 2015. Topography driven fluid flow within orogenic wedges: Effects of taper angle and depth-dependent permeability. Geosphere, 11(5), 1-11.

Puigdefàbregas, C., Muñoz, J.A. and Marzo, M., 1986. Thrust Belt Development in the Eastern Pyrenees and Related Depositional Sequences in the Southern Foreland Basin. In: P.A. Allen and P. Homewood (Eds.), Foreland Basins. Blackwell Publishing Ltd., Oxford, UK. , pp. 229-246.

Puigdefàbregas, C., Muñoz, J.A. and Vergés, J., 1992. Thrusting and Foreland Basin Evolution in the Southern Pyrenees. In: K.R. McClay (Ed.), Thrust Tectonics. London, Chapman & Hall, pp. 247-254.

Qing, H. and Mountjoy, E., 1992. Large-scale fluid flow in the Middle Devonian Presqu'ile barrier, Western Canada Sedimentary Basin. Geology, 20, 903-906.

Reynolds, S.J. and Lister, G.S., 1987. Structural aspects of fluid-rock interactions in detachment zones. Geology, 15, 362-366.

Rodríguez-Morillas, N., Playà, E., Travé, A. and Martín-Martín, J.D., 2013. Diagenetic processes in a partially dolomitized carbonate reservoir: Casablanca oil field, Mediterranean Sea, offshore Spain. Geologica Acta, 11(2), 195-214.

Rosell, J., Linares, R. and Llompart, C., 2001. El "Garumniense" prepirenaico. Rev. Soc. Geol. España, 14(1-2), 47-56.

Roure, F., Andriessen, P., Callot, J.P., Faure, J.L., Ferket, H., Gonzales, E., Guilhaumou, N., Lacombe, O., Malandain, J., Sassi, W., Schneider, F., Swennen, R. and Vilasi, N., 2010. The use of paleo-thermo-barometers and coupled thermal, fluid flow and pore-fluid pressure modelling for hydrocarbon and reservoir prediction in fold and thrust belts. In: G.P. Goffey, J. Craig, T. Needham and R. Scott (Eds.), Hydrocarbons in Contractional Belts. Geological Society, London, Special Publications, pp. 87-114.

Roure, F., Choukroune, P., Berastegui, J., Muñoz, J.A., Villien, A., Matheron, P., Bareyt, M., Seguret, M., Camara, P. and Deramond, J., 1989. Ecors deep seismic data and balanced cross sections: Geometric constraints on the evolution of the Pyrenees. Tectonics, 8(1), 41-50.

Roure, F., Swennen, R., Schneider, F., Faure, J.L., Ferket, H., Guilhaumou, N., Osadetz, K., Robion, P. and Vandeginste, V., 2005. Incidence and Importance of Tectonics and Natural Fluid Migration on Reservoir Evolution in Foreland Fold-and-Thrust Belts. Oil & Gas Science and Technology, 60(1), 67-106.

Sans, M., 2003. From thrust tectonics to diapirism. The role of evaporites in the kinematic evolution of the eastern South Pyrenean front. Geologica Acta, 1(3), 239-259.

Schneider, F., 2003. Basin Modeling in Complex Area: Examples from Eastern Venezuelan and Canadian Foothills. Oil & Gas Science and Technology, 58(2), 313-324.

Séguret, M., 1972. Étude tectonique des nappes et séries décollées de la partie centrale du vesant sud des Pyrénées. Pub. USTELA, sér, Geol. Struct. n.2, Montpellier, 155 pp.

Serra-Kiel, J., Hottinger, L., Caus, E., Drobne, K., Ferràndez, C., Jauhri, A.K., Less, G., Pavlovec, R., Pignatti, J., Samsó, J.M., Schaub, H., Sirel, E., Strougo, A., Tamberau, Y., Tosquella, J. and Zakrevskaya, E., 1998a. Larger Foraminiferal Biostratigraphy of the Tethyan Paleocene and Eocene. Bulletin de la Societé Géologique de France, 169(2), 281-299.

Serra-Kiel, J., Hottinger, L., Drobne, K., Ferràndez, C., Jauhri, A.K., Less, G., Pignatti, J., Samsó, J.M., Schaub, H., Sirel, E., Tamberau, Y., Tosquella, J. and Zakrevskaya, E., 1998b. Larger benthic Foraminifera In: J. Thierry, M.B. Farley, T. Jacquin, P.C. Graciansky and P.R. Vail

(Eds.), Mesozoic-Cenozoic sequence stratigraphy of European basins., Society of Economic Paleontologist and Mineralogist, Special Publication, pp. 60pp.

Serra-Kiel, J., Travé, A., Mató, E., Saula, E., Ferràndez-Cañadell, C., Busquets, P., Tosquella, J. and Vergés, J., 2003. Marine and Transitional Middle/Upper Eocene Units of the Southeastern Pyrenean Foreland Basin (NE Spain). Geologica Acta, 1(2), 177-200.

Shackleton, J.R., Cooke, M.L. and Sussman, A.J., 2005. Evidence for temporally changing mechanical stratigraphy and effects on joint-network architecture. Geology, 33(2), 101-104.

Sibson, R.H., Robert, F. and Poulsen, K.H., 1988. High-angle reverse faults, fluid-pressure cycling, and mesothermal gold-quartz deposits. Geology, 16, 551-555.

Swart, P.K., 2015. The geochemistry of carbonate diagenesis: The past, present and future. Sedimentology, 62(5), 1233-1304.

Swennen, R., Ferket, H., Benchilla, L., Roure, F., Ellam, R. and team, S., 2003. Fluid flow and diagenesis in carbonate dominated Foreland Fold and Thrust Belts: petrographic inferences from field studies of late-diagenetic fabrics from Albania, Belgium, Canada, Mexico and Pakistan. Journal of Geochemical Exploration, 78-79, 481-485.

Taylor, B.E., 1987. Stable isotope geochemistry of ore-forming fluids. In: T.K. Kyser (Ed.), Short Course in Stable Isotope Geochemistry of low Temperature Fluids. Mineral Association of Canada, pp. 337-418.

Tindall, J., Flecker, R., Valdes, P., Schmidt, D.N., Markwick, P. and Harris, J., 2010. Modelling the oxygen isotope distribution of ancient seawater using a coupled ocean–atmosphere GCM: Implications for reconstructing early Eocene climate. Earth and Planetary Science Letters, 292, 265-273.

Travé, A., Calvet, F., Salas, R. and Playà, E., 2004. Fluid Flow during Paleogene Compression in the Linking Zone Fold and Thrust Belt (Northeast Spain). In: R. Swennen, F. Roure and J.W. Granath (Eds.), Deformation, fluid flow, and reservoir appraisal in foreland fold and thrust belts. AAPG Hedberg Series, pp. 215-243.

Travé, A., Calvet, F., Sans, M., Vergés, J. and Thirlwall, M., 2000. Fluid history related to the Alpine compression at the margin of the south-Pyrenean Foreland basin: the El Guix anticline. Tectonophysics, 321, 73-102.

Travé, A., Labaume, P., Calvet, F. and Soler, A., 1997. Sediment dewatering and pore fluid migration along thrust faults in a foreland basin inferred from isotopic and elemental geochemical analyses (Eocene southern Pyrenees, Spain). Tectonophysics, 282(1-4), 375-398.

Travé, A., Labaume, P., Calvet, F., Soler, A., Tritlla, J., Bautier, M., Potdevin, J.L., Séguret, M., Raynaud, S. and Briqueu, L., 1998. Fluid migration during Eocene thrust emplacement in the south Pyrenean foreland basin (Spain): an integrated structural, mineralogical and geochemical approach. In: A. Mascle, C. Puigdefàbregas, H.P. LuterBacher and M. Fernàndez (Eds.), Cenozoic Foreland Basins of Western Europe. Geological Society, Special Publications, pp. 163-188.

Travé, A., Labaume, P. and Vergés, J., 2007. Fluid systems in Foreland Fold and thrust belts: an overview from the Southern Pyrenees. In: O. Lacombe, J. Lavé, F. Roure and J. Vergés (Eds.), Thrust Belts and Foreland Basins: From Fold Kinematics to Hydrocarbon Systems. Springer, pp. 93-115.

Tucker, M.E. and Wright, P.V., 1990. Carbonate Sedimentology. Blackwell, Oxford, 482 pp.

Valero, L., Garcés, M., Cabrera, L., Costa, E. and Sáez, A., 2014. 20 Myr of eccentricity paced lacustrine cycles in the Cenozoic Ebro Basin Earth and Planetary Science Letters, 408, 183-193.

Vandeginste, V., Swennen, R., Allaeys, M., Ellam, R.M., Osadetz, K. and Roure, F., 2012. Challenges of structural diagenesis in foreland fold-and-thrust belts: A case study on paleofluid flow in the Canadian Rocky Mountains West of Calgary. Marine and Petroleum Geology, 35(1), 235-251.

Vergés, J., 1993. Estudi geològic del vessant sud del Pirineu oriental i central. Evolució cinemàtica en 3D, PhD thesis, Universitat de Barcelona, Barcelona, Spain, 203 pp.

Vergés, J. and Burbank, D.W., 1996. Eocene-Oligocene thrusting and basin configuration in the eastern and central Pyrenees (Spain). In: P. Friend and C. Dabrio (Eds.), Tertiary basins of Spain. Cambridge University, World and Regional geology, E11, pp. 120-133.

Vergés, J., Fernàndez, M. and Martínez, A., 2002a. The Pyrenean orogen: pre-, syn-, and post-collisional evolution. In: G. Rosenbaum and G. Lister (Eds.), Reconstruction of the evolution of the Alpine-Himalayan Orogen. Journal of the Virtual Explorer, pp. 55-74.

Vergés, J., Martínez, A. and Muñoz, J.A., 1992. South Pyrenean fold and thrust belt: The role of foreland evaporitic levels in thrust geometry. In: K. McClay (Ed.), Thrust Tectonics. London, Chapman & Hall, pp. 255-264.

Vergés, J., Marzo, M. and Muñoz, J.A., 2002b. Growth strata in foreland settings. Sedimentary Geology, 146, 1-9.

Vergés, J., Marzo, M., Santaeulària, T., Serra-Kiel, J., Burbank, D.W., Muñoz, J.A. and Giménez-Montsant, J., 1998. Quantified vertical motions and tectonic evolution of the SE Pyrenean foreland basin. In: A. Mascle, C. Puigdefàbregas, H.P. Luterbacher and M. Fernàndez (Eds.), Cenozoic Foreland Basins of Western Europe. Geological Society Special Publications, pp. 107-134.

Vergés, J., Millán, H., Roca, E., Muñoz, J.A., Marzo, M., Cirés, J., Bezemer, T.D., Zoetemeijer, R. and Cloetigh, S., 1995. Eastern Pyrenees and related foreland basins: pre-, syn- and post-collisional cristal-scale cross-sections. Marine and Petroleum Geology, 12(8), 893-915.

Vergés, J. and Muñoz, J.A., 1990. Thrust sequences in the southern central Pyrenees. Bull. Soc. géol. France, 8(6), 265-271.

Vilasi, N., 2010. Study of reservoir analogues in foreland fold-and-thrust belts: sedimentology, diagenesis, deformation and fracturing of the upper cretaceous-eocene carbonate systems of the ionian zone (Southern Albania), PhD thesis. Ecole des Mines de Paris, Paris, France, 190 pp.

Vilasi, N., Malandain, J., Barrier, L., Callot, J.P., Amrouch, K., Guilhaumou, N., Lacombe, O., Muska, K., Roure, F. and Swennen, R., 2009. From outcrop and petrographic studies to basin-scale fluid flow modelling: The use of the Albanian natural laboratory for carbonate reservoir characterisation. Tectonophysics, 474, 367-392.

Warren, J.K., 2006. Evaporites:Sediments, Resources and Hydrocarbons. Springer Berlin Heidelberg.

Fig. 1

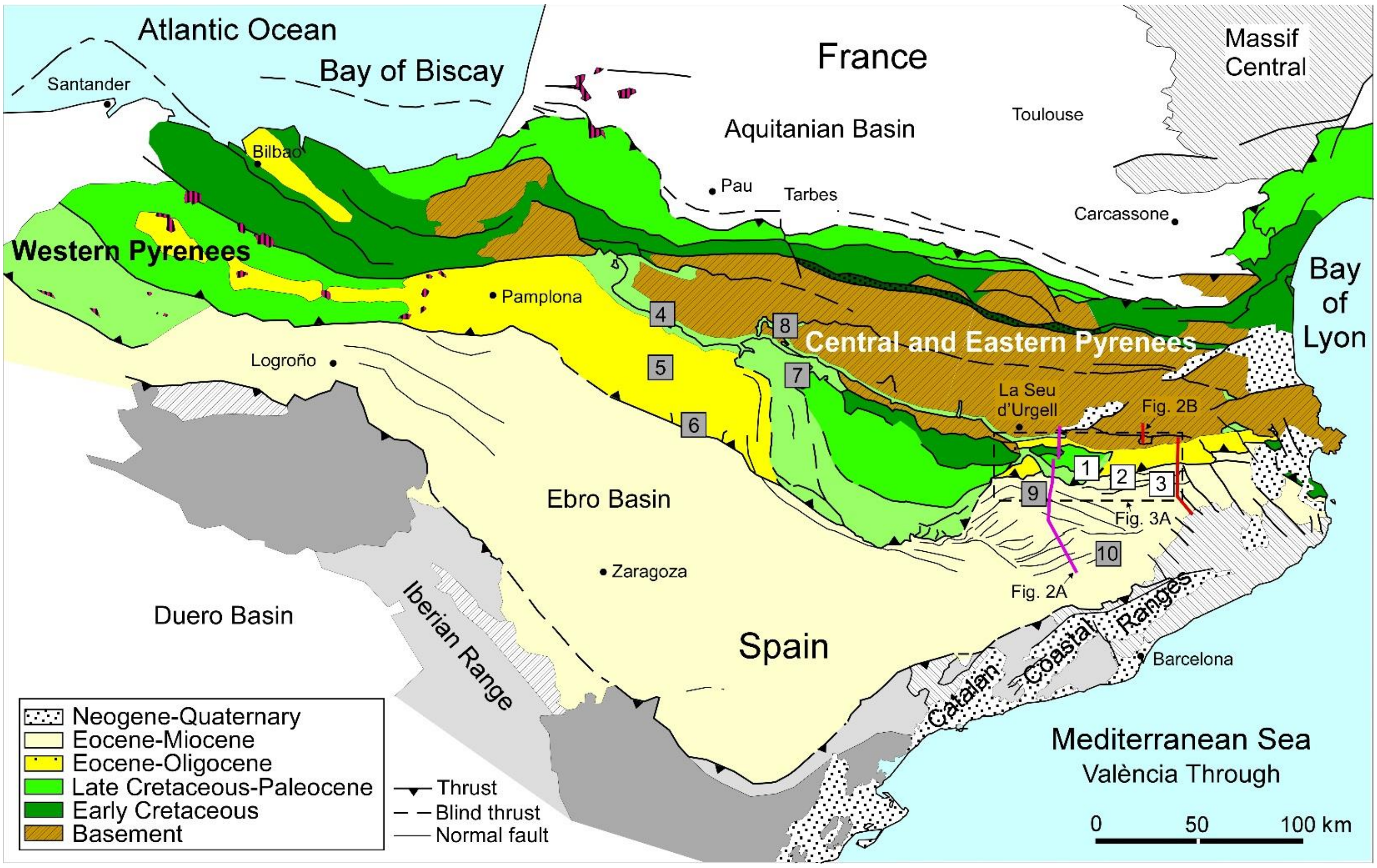

Atlantic Ocean
Bay of Biscay
France
Massif Central
Santander
Bilbao
Aquitanian Basin
Toulouse
Pau
Tarbes
Carcassone
Western Pyrenees
Bay of Lyon
Pamplona
Central and Eastern Pyrenees
Logroño
La Seu d'Urgell
Fig. 2B
Fig. 3A
Fig. 2A
Ebro Basin
Zaragoza
Duero Basin
Iberian Range
Spain
Catalan Coastal Ranges
Barcelona
Mediterranean Sea
València Through
1
2
3
4
5
6
7
8
9
10
Neogene-Quaternary
Eocene-Miocene
Eocene-Oligocene
Late Cretaceous-Paleocene
Early Cretaceous
Basement
Thrust
Blind thrust
Normal fault
0
50
100 km

Fig. 2

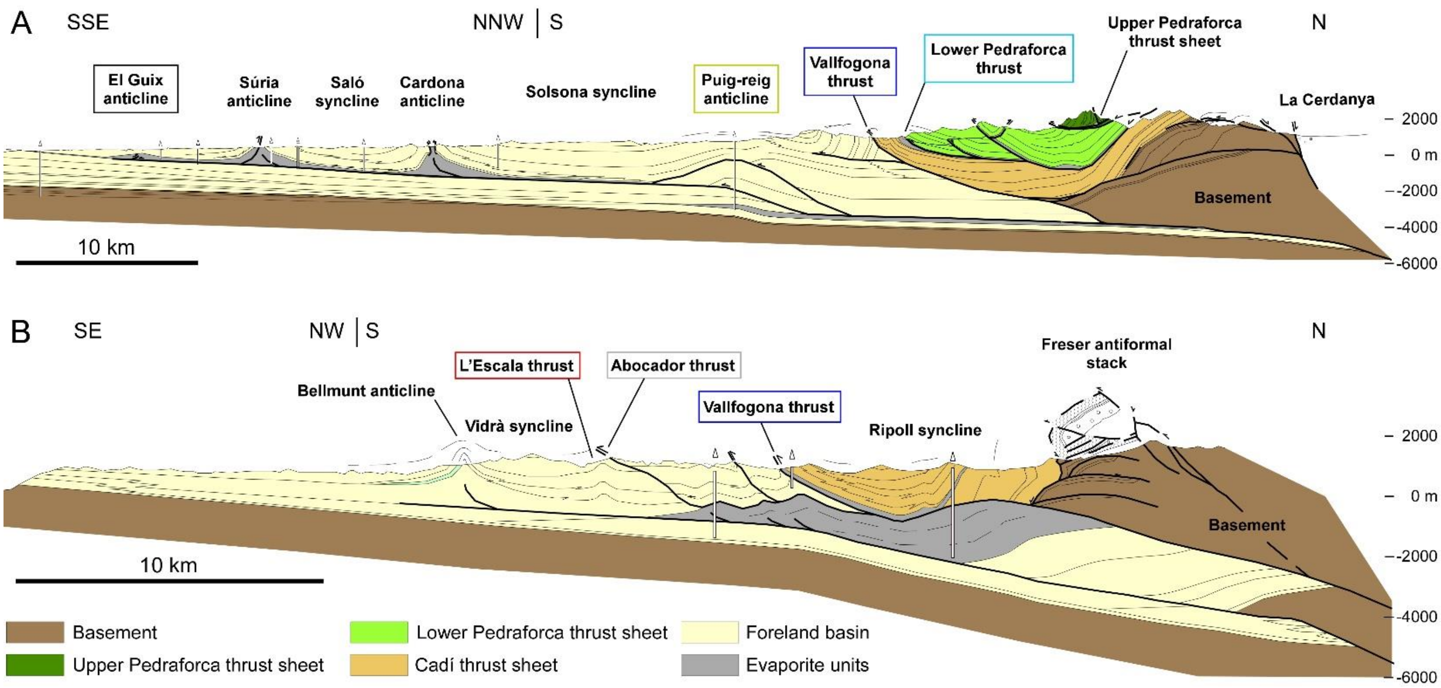

A
SSE
NNW
S
N
El Guix anticline
Súria anticline
Saló syncline
Cardona anticline
Solsona syncline
Puig-reig anticline
Vallfogona thrust
Lower Pedraforca thrust
Upper Pedraforca thrust sheet
La Cerdanya
Basement
10 km
2000
0 m
-2000
-4000
-6000
B
SE
NW
S
N
Bellmunt anticline
L'Escala thrust
Abocador thrust
Vidrà syncline
Vallfogona thrust
Ripoll syncline
Freser antiformal stack
Basement
10 km
2000
0 m
-2000
-4000
-6000
Basement
Upper Pedraforca thrust sheet
Lower Pedraforca thrust sheet
Cadí thrust sheet
Foreland basin
Evaporite units

Fig. 3

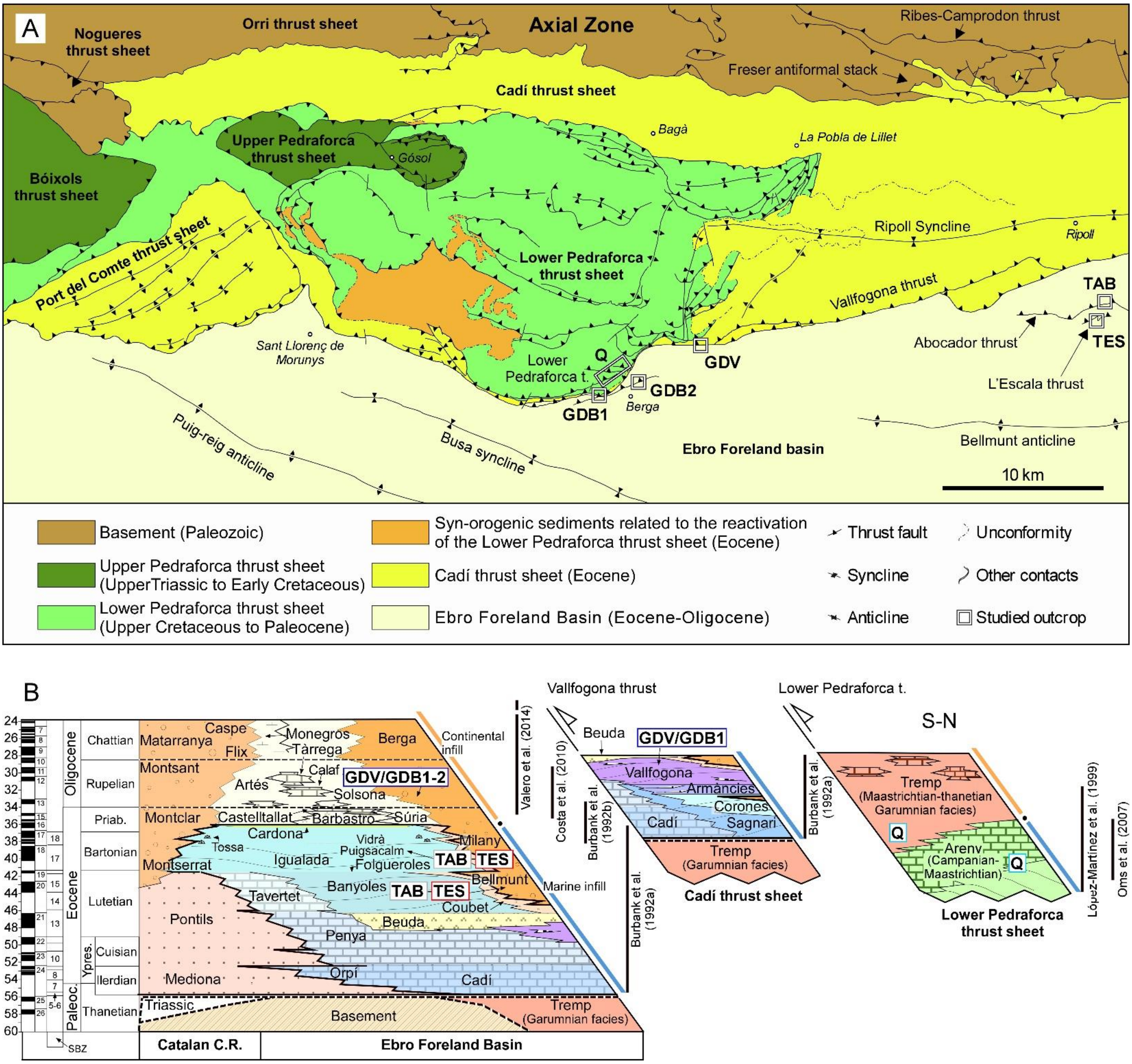
A
Nogueres thrust sheet
Orri thrust sheet
Axial Zone
Ribes-Camprodon thrust
Freser antiformal stack
Cadí thrust sheet
Upper Pedraforca thrust sheet
Gósol
Bagà
La Pobla de Lillet
Bóixols thrust sheet
Port del Comte thrust sheet
Lower Pedraforca thrust sheet
Ripoll Syncline
Ripoll
Vallfogona thrust
TAB
TES
Abocador thrust
L'Escala thrust
Sant Llorenç de Morunys
Lower Pedraforca t.
Q
GDV
GDB2
GDB1
Berga
Puig-reig anticline
Busa syncline
Ebro Foreland basin
Bellmunt anticline
10 km
Basement (Paleozoic)
Upper Pedraforca thrust sheet (UpperTriassic to Early Cretaceous)
Lower Pedraforca thrust sheet (Upper Cretaceous to Paleocene)
Syn-orogenic sediments related to the reactivation of the Lower Pedraforca thrust sheet (Eocene)
Cadí thrust sheet (Eocene)
Ebro Foreland Basin (Eocene-Oligocene)
Thrust fault
Syncline
Anticline
Unconformity
Other contacts
Studied outcrop
B
Oligocene
Eocene
Paleoc.
Chattian
Rupelian
Priab.
Bartonian
Lutetian
Ypres.
Cuisian
Ilerdian
Thanetian
SBZ
Catalan C.R.
Ebro Foreland Basin
Caspe
Matarranya
Flix
Monegros
Tàrrega
Berga
Montsant
Artés
Calaf
Solsona
GDV/GDB1-2
Montclar
Castelltallat
Barbastro
Súria
Cardona
Tossa
Igualada
Vidrà
Puigsacalm
Folgueroles
Milany
Montserrat
TAB
TES
Bellmunt
Banyoles
Tavertet
Coubet
Pontils
Beuda
Penya
Mediona
Orpí
Cadí
Triassic
Basement
Tremp (Garumnian facies)
Continental infill
Marine infill
Valero et al. (2014)
Costa et al. (2010)
Burbank et al. (1992b)
Burbank et al. (1992a)
Vallfogona thrust
Beuda
GDV/GDB1
Vallfogona
Armàncies
Corones
Sagnari
Cadí
Tremp (Garumnian facies)
Cadí thrust sheet
Lower Pedraforca t.
S-N
Tremp (Maastrichtian-thanetian Garumnian facies)
Q
Arenv (Campanian-Maastrichtian)
Lower Pedraforca thrust sheet
López-Martinez et al. (1999)
Oms et al. (2007)

Fig. 4

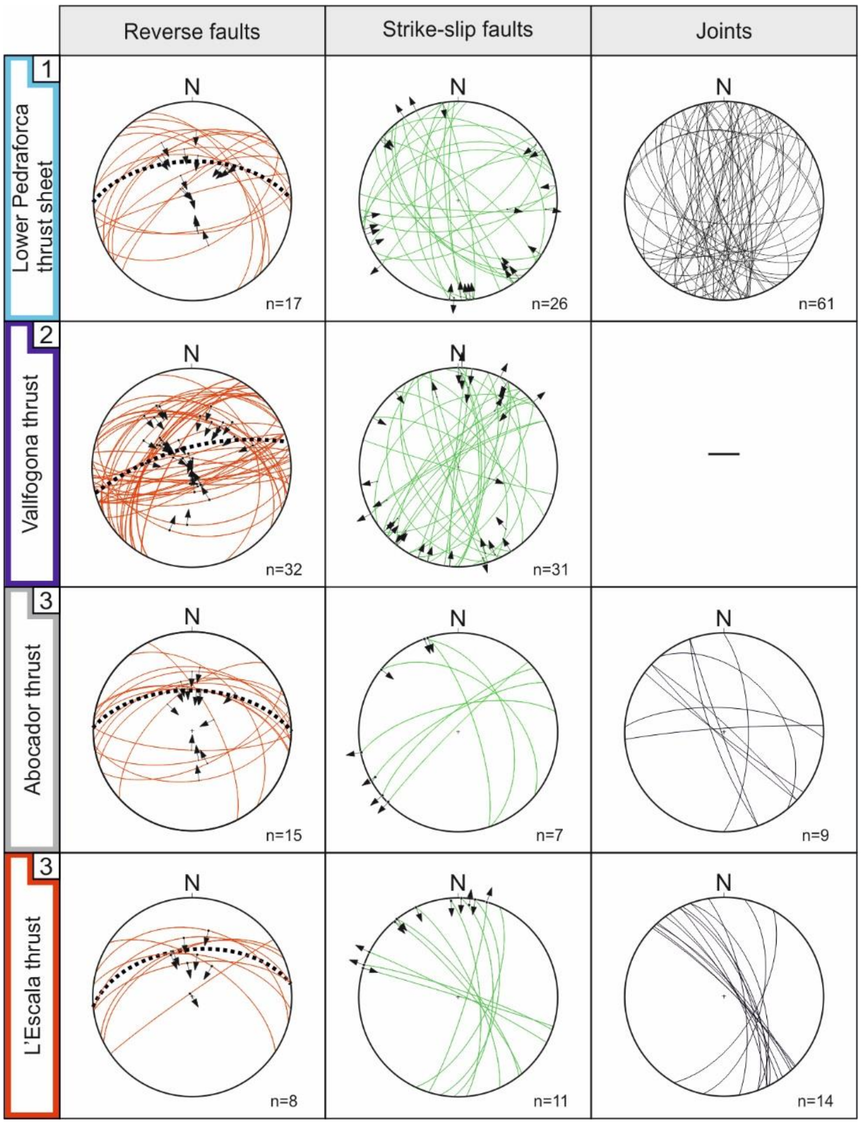

Reverse faults
Strike-slip faults
Joints
1
Lower Pedraforca thrust sheet
2
Vallfogona thrust
3
Abocador thrust
3
L'Escala thrust
N
n=17
n=26
n=61
n=32
n=31
—
n=15
n=7
n=9
n=8
n=11
n=14

993 Fig. 5

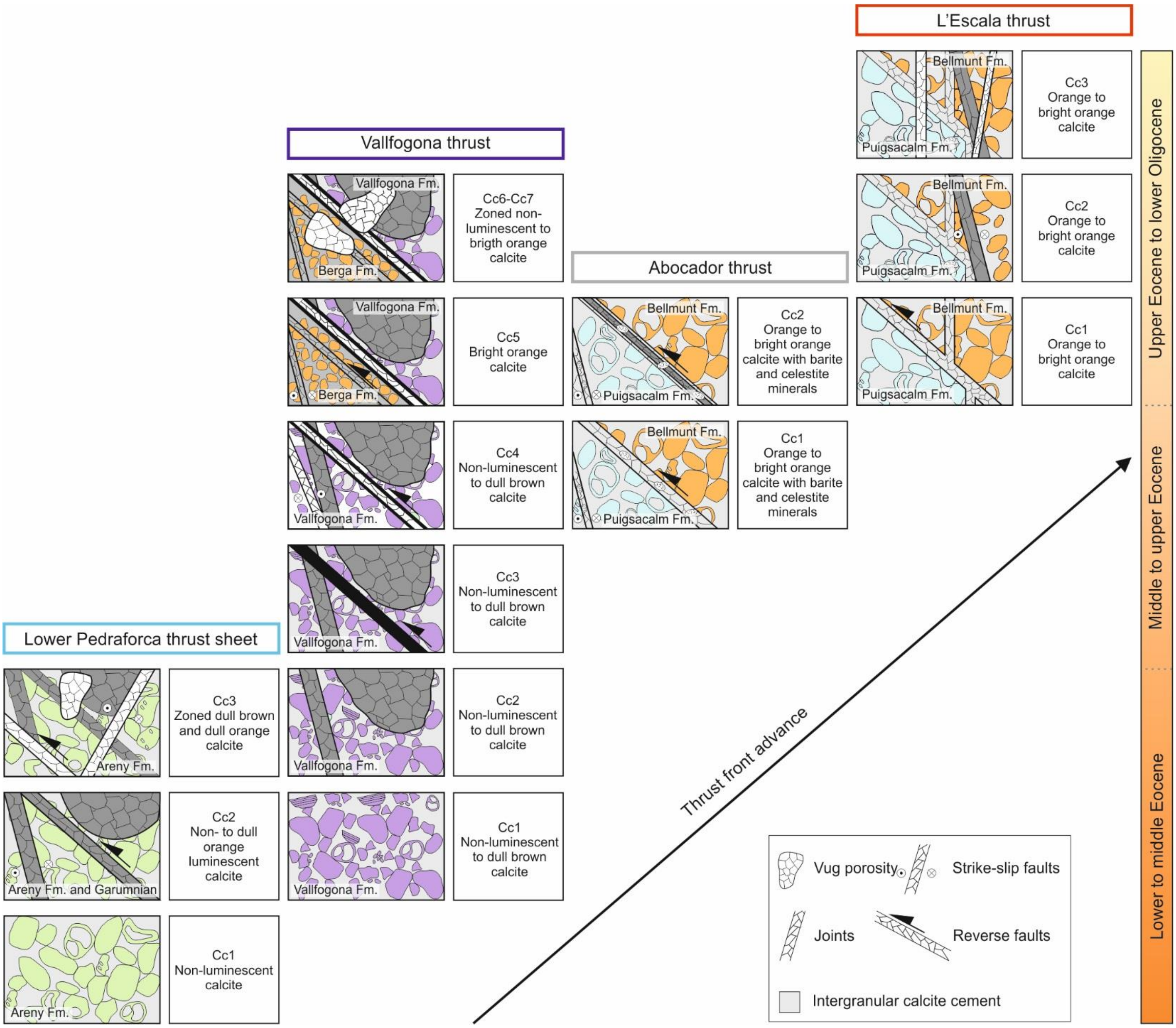

L'Escala thrust
Vallfogona thrust
Abocador thrust
Lower Pedraforca thrust sheet
Bellmunt Fm.
Puigsacalm Fm.
Vallfogona Fm.
Berga Fm.
Areny Fm.
Areny Fm. and Garumnian
Cc3 Orange to bright orange calcite
Cc2 Orange to bright orange calcite
Cc1 Orange to bright orange calcite
Cc6-Cc7 Zoned non-luminescent to brigth orange calcite
Cc5 Bright orange calcite
Cc4 Non-luminescent to dull brown calcite
Cc3 Non-luminescent to dull brown calcite
Cc2 Non-luminescent to dull brown calcite
Cc1 Non-luminescent to dull brown calcite
Cc2 Orange to bright orange calcite with barite and celestite minerals
Cc1 Orange to bright orange calcite with barite and celestite minerals
Cc3 Zoned dull brown and dull orange calcite
Cc2 Non- to dull orange luminescent calcite
Cc1 Non-luminescent calcite
Thrust front advance
Vug porosity
Strike-slip faults
Joints
Reverse faults
Intergranular calcite cement
Upper Eocene to lower Oligocene
Middle to upper Eocene
Lower to middle Eocene

994

Fig. 6

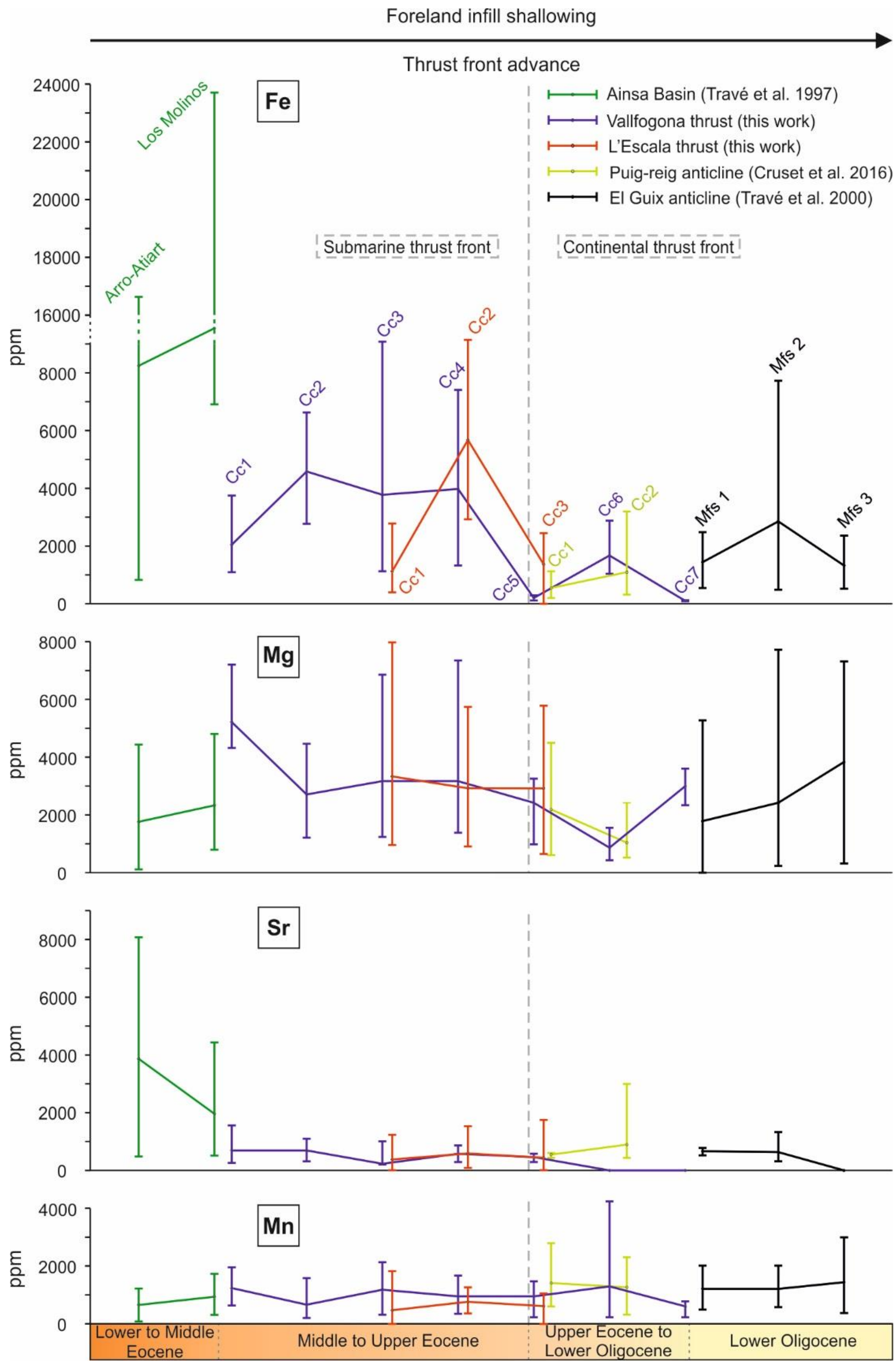

Foreland infill shallowing
Thrust front advance
Fe
Mg
Sr
Mn
ppm
Ainsa Basin (Travé et al. 1997)
Vallfogona thrust (this work)
L'Escala thrust (this work)
Puig-reig anticline (Cruset et al. 2016)
El Guix anticline (Travé et al. 2000)
Submarine thrust front
Continental thrust front
Los Molinos
Arro-Atiart
Cc1
Cc2
Cc3
Cc4
Cc5
Cc6
Cc7
Mfs 1
Mfs 2
Mfs 3
Lower to Middle Eocene
Middle to Upper Eocene
Upper Eocene to Lower Oligocene
Lower Oligocene

Fig. 7

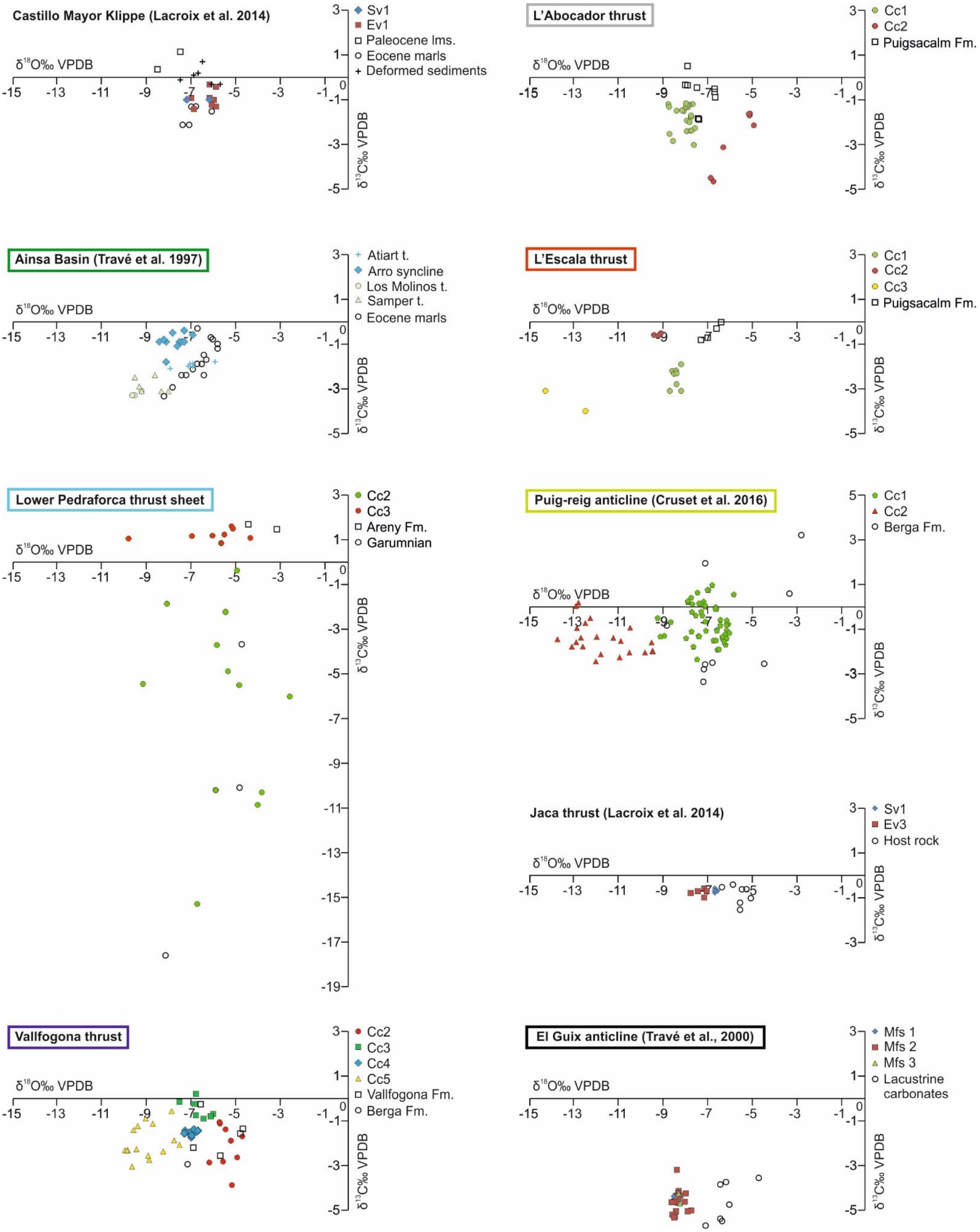

Castillo Mayor Klippe (Lacroix et al. 2014)
Sv1
Ev1
Paleocene lms.
Eocene marls
Deformed sediments
L'Abocador thrust
Cc1
Cc2
Puigsacalm Fm.
Ainsa Basin (Travé et al. 1997)
Atiart t.
Arro syncline
Los Molinos t.
Samper t.
Eocene marls
L'Escala thrust
Cc1
Cc2
Cc3
Puigsacalm Fm.
Lower Pedraforca thrust sheet
Cc2
Cc3
Areny Fm.
Garumnian
Puig-reig anticline (Cruset et al. 2016)
Cc1
Cc2
Berga Fm.
Jaca thrust (Lacroix et al. 2014)
Sv1
Ev3
Host rock
Vallfogona thrust
Cc2
Cc3
Cc4
Cc5
Vallfogona Fm.
Berga Fm.
El Guix anticline (Travé et al., 2000)
Mfs 1
Mfs 2
Mfs 3
Lacustrine carbonates
δ18O‰ VPDB
δ13C‰ VPDB

Fig. 8

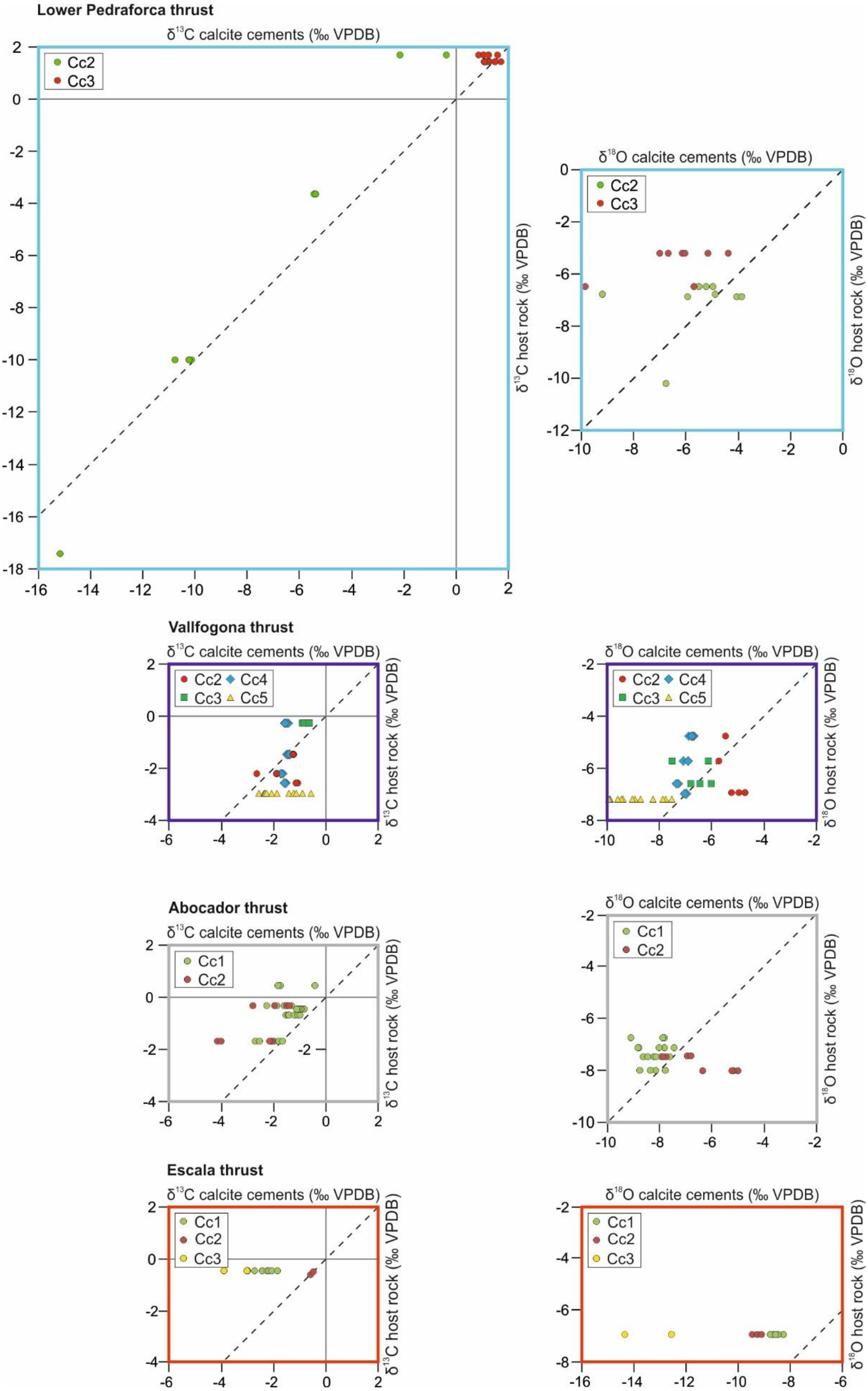

Lower Pedraforca thrust
δ13C calcite cements (‰ VPDB)
δ13C host rock (‰ VPDB)
Cc2
Cc3
δ18O calcite cements (‰ VPDB)
δ18O host rock (‰ VPDB)
Cc2
Cc3
Vallfogona thrust
δ13C calcite cements (‰ VPDB)
δ13C host rock (‰ VPDB)
Cc2 Cc4
Cc3 Cc5
δ18O calcite cements (‰ VPDB)
δ18O host rock (‰ VPDB)
Cc2 Cc4
Cc3 Cc5
Abocador thrust
δ13C calcite cements (‰ VPDB)
δ13C host rock (‰ VPDB)
Cc1
Cc2
δ18O calcite cements (‰ VPDB)
δ18O host rock (‰ VPDB)
Cc1
Cc2
Escala thrust
δ13C calcite cements (‰ VPDB)
δ13C host rock (‰ VPDB)
Cc1
Cc2
Cc3
δ18O calcite cements (‰ VPDB)
δ18O host rock (‰ VPDB)
Cc1
Cc2
Cc3

Fig. 9

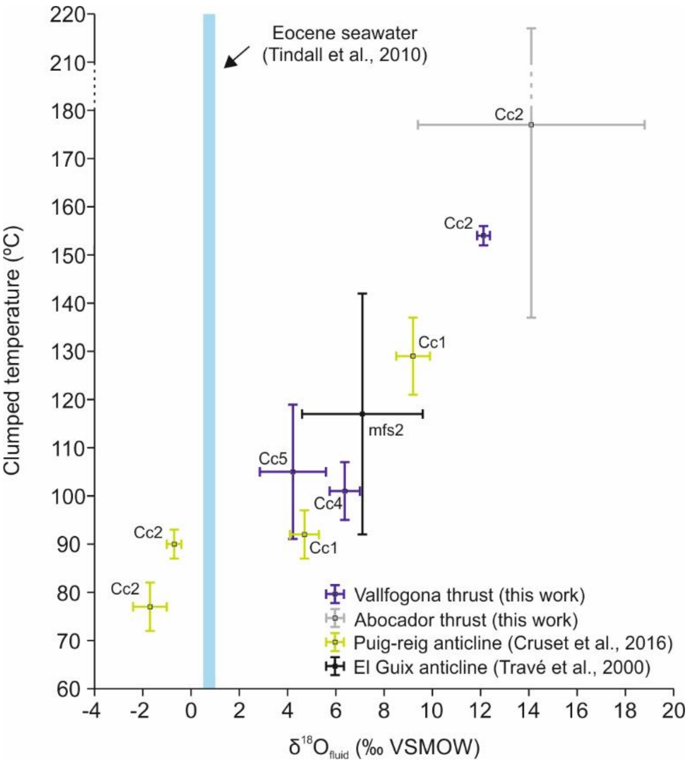
Eocene seawater
(Tindall et al., 2010)
Clumped temperature (ºC)
δ18Ofluid (‰ VSMOW)
Cc2
Cc2
Cc1
mfs2
Cc5
Cc4
Cc1
Cc2
Cc2
Vallfogona thrust (this work)
Abocador thrust (this work)
Puig-reig anticline (Cruset et al., 2016)
El Guix anticline (Travé et al., 2000)
220
210
180
170
160
150
140
130
120
110
100
90
80
70
60
-4
-2
0
2
4
6
8
10
12
14
16
18
20

.006 Fig. 10

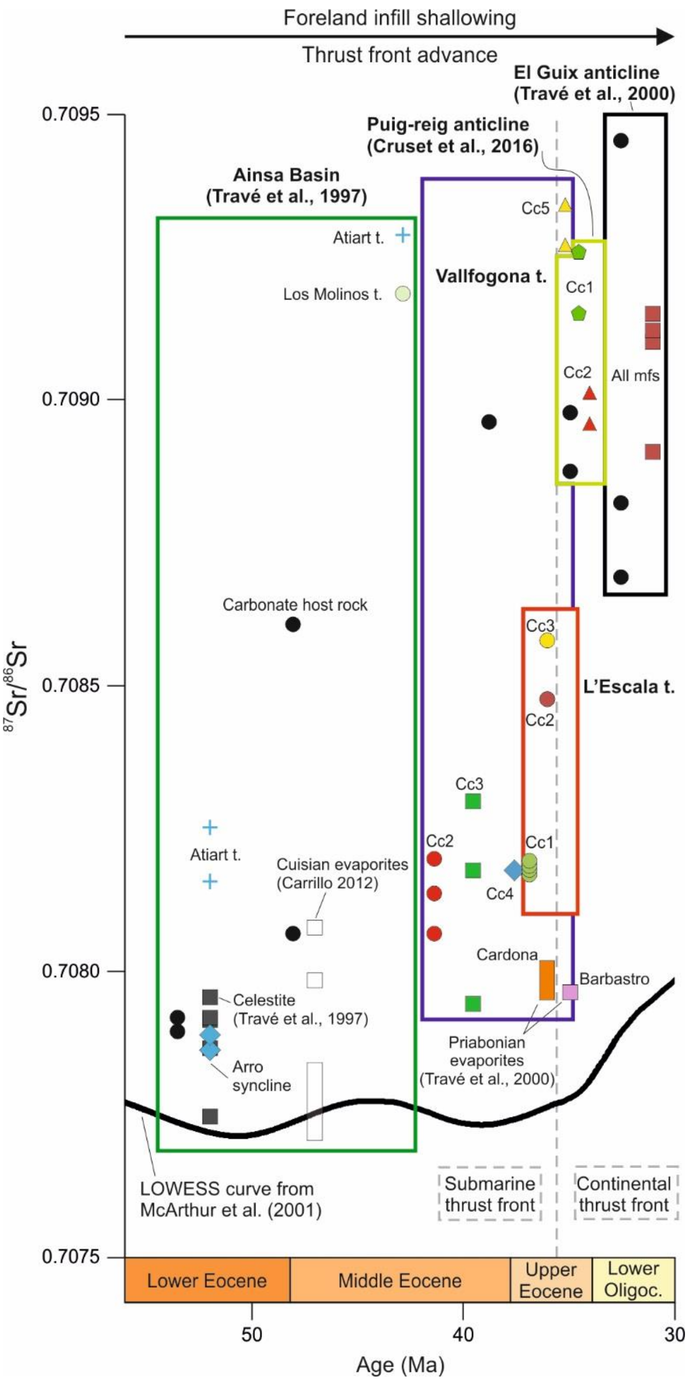

.007

Fig. 11

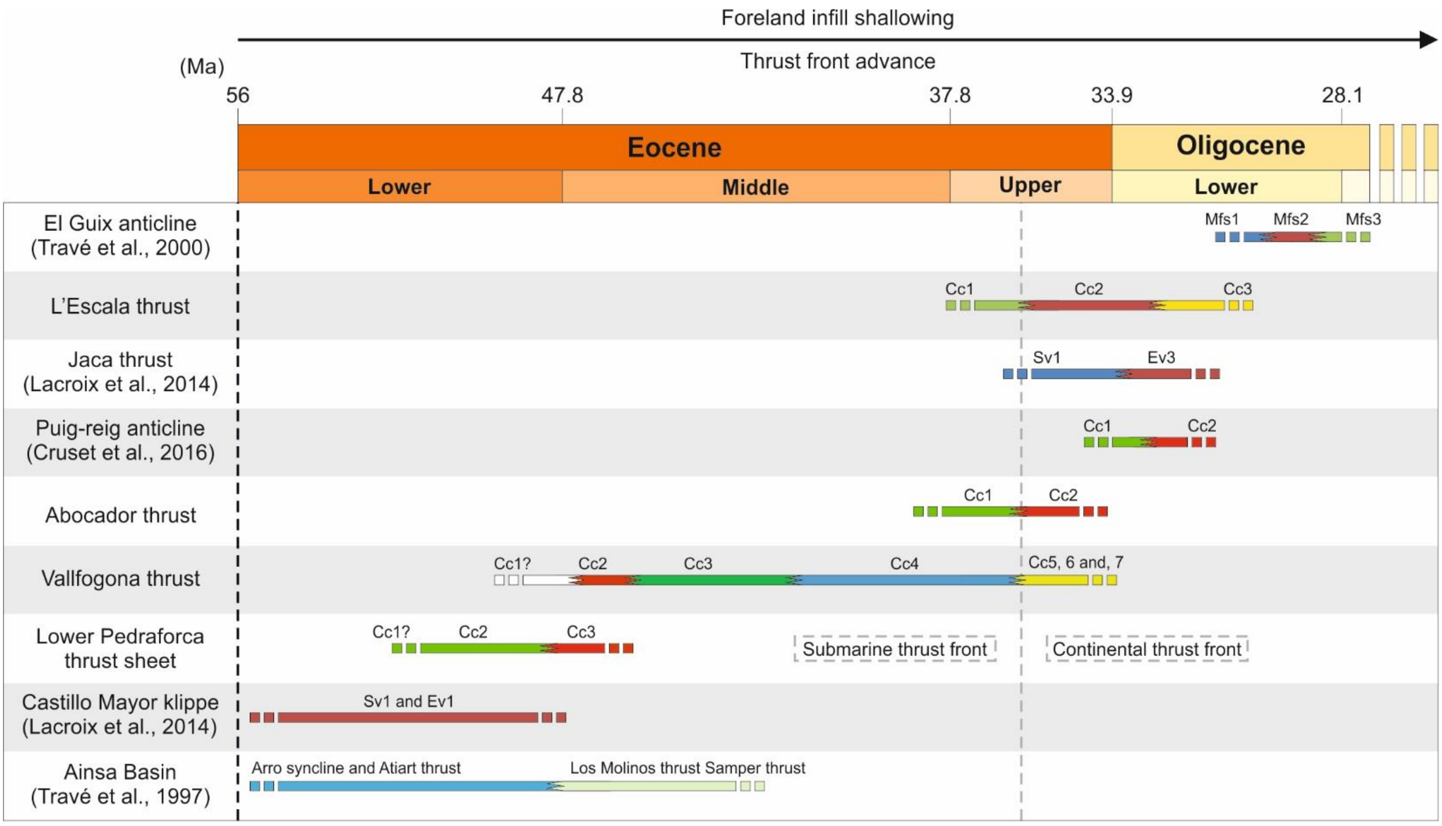
Foreland infill shallowing
Thrust front advance
(Ma)
56
47.8
37.8
33.9
28.1
Eocene
Oligocene
Lower
Middle
Upper
Lower
El Guix anticline (Travé et al., 2000)
Mfs1
Mfs2
Mfs3
L'Escala thrust
Cc1
Cc2
Cc3
Jaca thrust (Lacroix et al., 2014)
Sv1
Ev3
Puig-reig anticline (Cruset et al., 2016)
Cc1
Cc2
Abocador thrust
Cc1
Cc2
Vallfogona thrust
Cc1?
Cc2
Cc3
Cc4
Cc5, 6 and, 7
Lower Pedraforca thrust sheet
Cc1?
Cc2
Cc3
Submarine thrust front
Continental thrust front
Castillo Mayor klippe (Lacroix et al., 2014)
Sv1 and Ev1
Ainsa Basin (Travé et al., 1997)
Arro syncline and Atiart thrust
Los Molinos thrust Samper thrust

Fig. 12

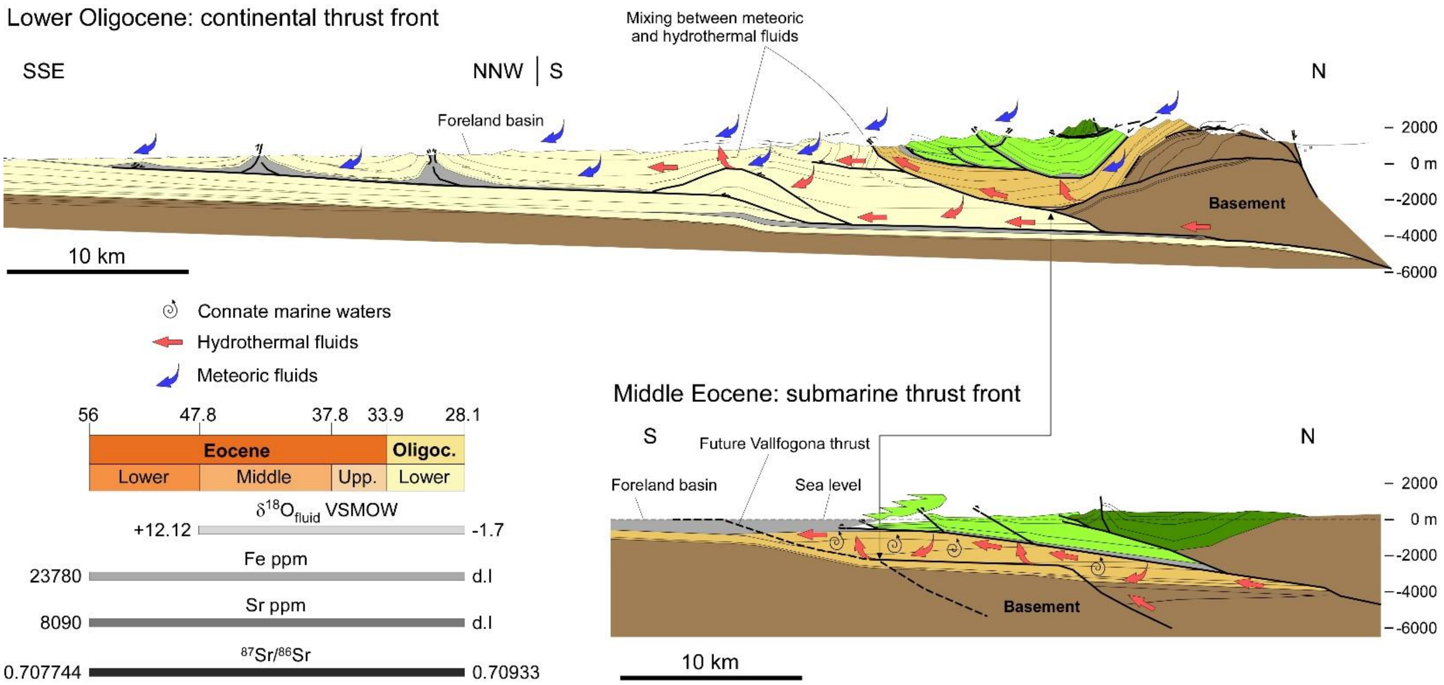

Lower Oligocene: continental thrust front
Mixing between meteoric and hydrothermal fluids
SSE
NNW
S
N
Foreland basin
Basement
2000
0 m
-2000
-4000
-6000
10 km
Connate marine waters
Hydrothermal fluids
Meteoric fluids
56
47.8
37.8
33.9
28.1
Eocene
Oligoc.
Lower
Middle
Upp.
Lower
$\delta^{18}O_{fluid}$ VSMOW
+12.12
-1.7
Fe ppm
23780
d.l
Sr ppm
8090
d.l
$^{87}Sr/^{86}Sr$
0.707744
0.70933
Middle Eocene: submarine thrust front
S
N
Future Vallfogona thrust
Foreland basin
Sea level
Basement
2000
0 m
-2000
-4000
-6000
10 km

Fig. 13

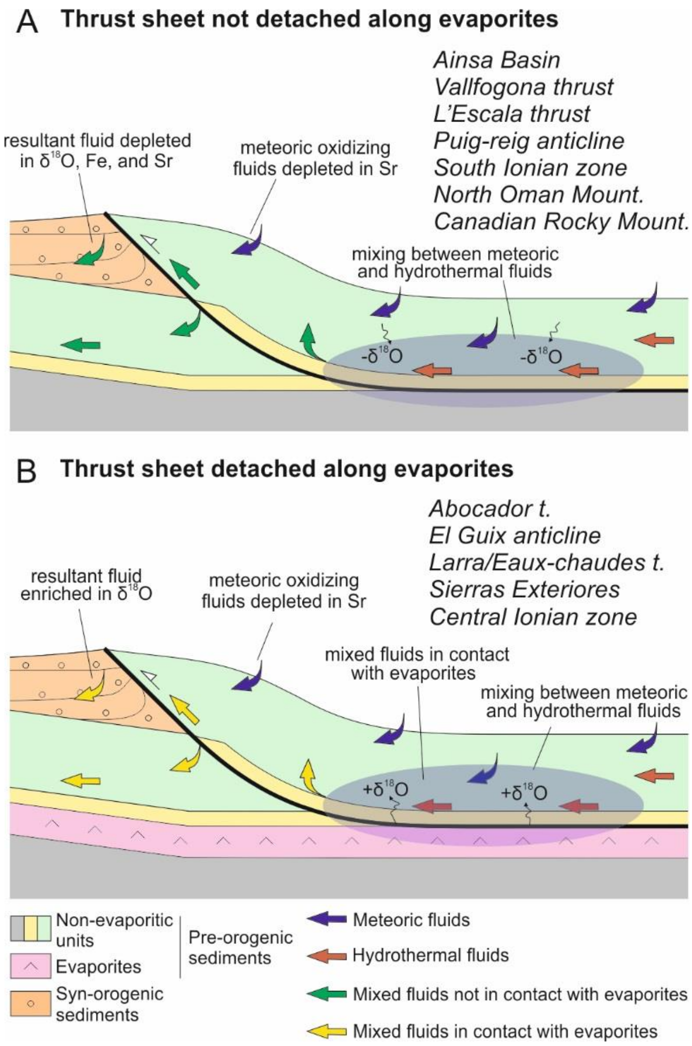
A Thrust sheet not detached along evaporites
Ainsa Basin
Vallfogona thrust
L'Escala thrust
Puig-reig anticline
South Ionian zone
North Oman Mount.
Canadian Rocky Mount.
resultant fluid depleted in δ18O, Fe, and Sr
meteoric oxidizing fluids depleted in Sr
mixing between meteoric and hydrothermal fluids
-δ18O
-δ18O
B Thrust sheet detached along evaporites
Abocador t.
El Guix anticline
Larra/Eaux-chaudes t.
Sierras Exteriores
Central Ionian zone
resultant fluid enriched in δ18O
meteoric oxidizing fluids depleted in Sr
mixed fluids in contact with evaporites
mixing between meteoric and hydrothermal fluids
+δ18O
+δ18O
Non-evaporitic units
Evaporites
Pre-orogenic sediments
Syn-orogenic sediments
Meteoric fluids
Hydrothermal fluids
Mixed fluids not in contact with evaporites
Mixed fluids in contact with evaporites

Fig. 1 Structural sketch of the Pyrenees from Vergés (1993). The white squares show the location of the studied structures in this work: 1) Lower Pedraforca thrust sheet; 2) Vallfogona thrust; 3) Abocador and L'Escala thrusts. The grey squares show the location of the structures previously studied by other authors that have been compared with our structures: 4) Larra/Eaux-chaudes thrust (Crognier et al., 2017); 5) Jaca Basin (Lacroix, et al., 2014; Crognier et al., 2017); 6) Sierras Exteriores (Beaudoin et al., 2015; Crognier, 2016); 7) Ainsa Basin (Travé et al., 1997); 8) Gavarnie thrust (McCaig et al., 1995); 9) Puig-reig anticline (Cruset et al., 2016); 10) El Guix anticline (Travé et al., 2000). The purple and red lines indicate the location of cross-sections shown in Figs. 2a and b, respectively.

Fig. 2 Cross sections of the studied areas (Vergés, 1993). The color boxes indicate the structural position of the studied outcrops in SE Pyrenees also shown in Fig. 1. Each color is equivalent to the color of lines and boxes in Figs. 3, 4, 5, 6, 7, 8, 9 and 10.

Fig. 3 A) Structural sketch of the studied area with outcrop locations. Q samples are referred to the Lower Pedraforca thrust sheet, GDV and GDB to the Vallfogona thrust and TAB and TES to the Abocador and L'Escala thrusts, respectively. B) N-S stratigraphic panel of the Lower Pedraforca thrust sheet, Cadí thrust sheet and eastern Ebro Foreland Basin modified from Vergés et al. (1998). The age of sedimentary units has been defined according to Burbank et al. (1992a, b), López-Martínez et al. (1999), Oms et al. (2007), Costa et al. (2010) and Valero et al. (2014). Shallow Benthic Zones (SBZ) from Serra-Kiel et al. (1998a and b). The color boxes with references Q, GDV, GDB, TAB and TES indicate the stratigraphic location of the studied outcrops.

Fig. 4 Lower hemisphere Schmidt stereoplots representing fracture data from the different studied outcrops. The dotted thick black lines indicate the main plane orientation for thrust faults. The boxes with numbers represent the structure location in Fig. 1.

Fig. 5 Cross-cutting relationships between fractures and related calcite cements in the Lower Pedraforca thrust sheet and Vallfogona, Abocador and L'Escala thrusts. The different cement generations and their main petrographic features as well as host rock formations are indicated.

Fig. 6 Elemental composition of the calcite cements for the Vallfogona and L'Escala thrusts, Ainsa Basin (Travé et al., 1997), El Guix anticline (Travé et al., 2000) and Puig-reig anticline (Cruset et al., 2016). For each structure Mg, Mn, Fe and Sr minimum, maximum and mean contents are given. Each of the different color lines represent one single structure. Equivalent colors are used in figures 2, 3, 4, 5, 7, 8, 9 and 10. The dashed grey line indicates the change from marine to continental conditions of thrust emplacement. The age of each calcite cement generation is approximated.

Fig. 7 $\delta^{18}O$ vs $\delta^{13}C$ cross-plots of carbonate host rocks and calcite cements from the Lower Pedraforca thrust sheet, Vallfogona, Abocador and L'Escala thrusts, Ainsa Basin (Travé et al., 1997), Castillo Mayor klippe and Jaca thrust (Lacroix et al., 2014), El Guix anticline (Travé et al., 2000) and Puig-reig anticline (Cruset et al., 2016). Empty symbols represent the different host rocks.

Fig. 8 $\delta^{13}C_{\text{calcite veins}}$ vs $\delta^{13}C_{\text{host rocks}}$ and $\delta^{18}O_{\text{calcite veins}}$ vs $\delta^{18}O_{\text{host rocks}}$ cross-plots from the Lower Pedraforca thrust sheet, Vallfogona, Abocador and L'Escala thrusts. The dashed black line represents the equilibrium between calcite veins and their adjacent host rocks.

Fig. 9 Clumped isotopes temperatures (°C) vs calculated $\delta^{18}O_{\text{fluid}}$ (‰ VSMOW) for The Vallfogona and Abocador thrusts, Puig-reig anticline (Cruset et al., 2016) and El Guix anticline (Travé et al., 2000). $\delta^{18}O$ Eocene seawater in ‰ VSMOW is from Tindall et al. (2010).

Fig. 10 $^{87}Sr/^{86}Sr$ composition of calcite cements, carbonate host rocks and celestite minerals from the Vallfogona and L'Escala thrusts, Ainsa Basin (Travé et al., 1997), El Guix anticline (Travé et al., 2000) and Puig-reig anticline (Cruset et al., 2016). The age of each calcite cement generation is approximated. The $^{87}Sr/^{86}Sr$ ratios of the Cuisian evaporites of the eastern sector of the south Pyrenean foreland basin from Carrillo (2012) and the LOWESS curve from McArthur et al. (2001)

are also plotted. The dashed grey line indicates the change from marine to continental conditions of thrust emplacement.

Fig. 11 Chronogram of the approximate ages of the different calcite cements in the Lower Pedraforca thrust sheet, Vallfogona, Abocador and L'Escala thrusts, Ainsa Basin (Travé et al., 1997), Castillo Mayor klippe and Jaca thrust (Lacroix et al., 2014), El Guix anticline (Travé et al., 2000) and Puig-reig anticline (Cruset et al., 2016). The dashed grey line indicates the change from marine to continental conditions of thrust emplacement.

Fig. 12 Fluid flow evolution in the south Pyrenean fold and thrust belt from submarine to continental conditions during thrust front emplacement. The shifts in $\delta^{18}O_{fluid}$ VSMOW, Fe and Sr content and $^{87}Sr/^{86}Sr$ ratio from Lower Eocene to Lower Oligocene are also included. The middle Eocene stage is redrawn from Vergés et al. (1995) and the lower Oligocene stage is redrawn from Vergés (1993). Legend units are in Fig. 2.

Fig. 13 Sketches of two possible scenarios for fluid flow regime in fold and thrust belts. A) Thrust sheet not detached through evaporites. B) Thrust sheet detached through evaporites. Not to scale.

Table 1

Structure	Sample	Cement type	n	$\delta^{13}C$ VPDB	$\delta^{18}O$ VPDB	Δ_{47}	T °C	$\delta^{18}O_{fluid}$ VSMOW
Vallfogona thrust	GDV20	Cc2	3	-1.06	-6.04	0.463 ± 0.002	154 ± 2	+12.12 ± 0.1434
	GDV30	Cc4	3	-1.66	-7.11	0.532 ± 0.010	101 ± 6	+6.37 ± 0.626
	GDV13	Cc5	3	-2.29	-9.64	0.527 ± 0.023	105 ± 14	+4.22 ± 1.37
Puig-reig anticline (Cruset et al., 2016)	309B1	Cc1	3	-0.44	-7.77	0.548 ± 0.009	92 ± 5	+4.7 ± 0.6
	317	Cc1	3	-0.99	-6.95	0.494 ± 0.010	129 ± 8	+9.2 ± 0.7
	311A	Cc2	3	-0.77	-12.32	0.574 ± 0.010	77 ± 5	-1.7 ± 0.7
	311D	Cc2	3	-0.73	-12.85	0.551 ± 0.004	90 ± 3	-0.7 ± 0.3
Abocador thrust	TAB9	Cc2	1	-1.69	-8.22	0.423 ± 0.03	177 ± 40	+14.1 ± 4,7
El Guix anticline	STn(3)(2)	Mfs2	1	-4.48	-8.62	0.487 ± 0.03	117 ± 25	+7.1 ± 2.5

Table 1 Calcite cement $\delta^{13}C$, $\delta^{18}O$, Δ_{47} and $\delta^{18}O_{fluid}$ of the Vallfogona thrust and Puig-reig anticline. Preliminary Δ_{47} and $\delta^{18}O_{fluid}$ for the Abocador thrust and El Guix anticline are also included. n represents the number of analyses per sample.